Technical Letter Report

TLR-RES/DE/REB-2023-03

Literature Review & Identification of System Performance Failure Modes Pertinent to CISCC Evolution and Risk Sequence

Date:

February 22, 2023

Prepared in response to Task 3B in User Need Request NMSS-2021-004, by:

R. D. Torres
Formerly U.S. Nuclear Regulatory Commission

Hector Mendoza
Sandia National Laboratories

NRC Project Manager:

Austin Young
Materials Engineer
Reactor Engineering Branch

Division of Engineering
Office of Nuclear Regulatory Research
U.S. Nuclear Regulatory Commission
Washington, DC 20555–0001

DISCLAIMER

This report does not contain or imply legally binding requirements. Nor does this report establish or modify any regulatory guidance or positions of the U.S. Nuclear Regulatory Commission and is not binding on the Commission.

EXECUTIVE SUMMARY

This report documents a scoping study that identifies and compiles the current state of knowledge on the susceptibility of dry storage systems for spent nuclear fuel to chloride-induced stress corrosion cracking (CISCC). This study identifies system performance failure modes pertinent to the potential evolution and risk sequence of CISCC in representative scenarios. Furthermore, the study compiles existing data, and models, and provides an assessment of data gaps to validate and verify the mechanistic or hybrid mechanistic/probabilistic sub-models to predict canister performance. A discussion is presented on the current understanding of CISCC with the relevant sub-models needed to capture key phenomena in existing spent fuel storage installations that could lead to stress corrosion cracking. The discussion presents past and ongoing works that investigate the conditions that lead to corrosion and subsequent cracking once corrosion initiates.

Critical models identified for CISCC can be categorized into four macroscopic stages: Onset of corrosion, crack initiation, crack growth, and mitigation. Mechanistic, probabilistic, or a hybrid set of approaches can be used to model each of the stages. Work by the Electric Power Research Institute (EPRI) has shown that a purely probabilistic approach for corrosion and flaw initiation requires estimated probabilities of initiation based on canister and storage site conditions. Work by Sandia National Laboratories (SNL) using a mechanistic-probabilistic (hybrid) approach to corrosion and crack initiation has highlighted that key input parameters for corrosion and flaw initiation include canister properties as well as the environmental parameters to which canisters are exposed. Models that capture growth for initiated cracks have a dependency on environmental conditions as well as on the stress distributions around flaw sites. An example of a simplified but common model used is the Wu and Modarres model. A version of this model is implemented in the EPRI and SNL approaches, where the model is calibrated with experimental data for relevant conditions. When the inspection stage is considered at storage sites, mitigation of stress corrosion cracks can be potentially be achieved. EPRI has shown that inspections and mitigation can be probabilistically modeled if a probability of detection is considered and identified for a scenario of interest.

The SNL model is identified as a tool that can simulate CISCC progression for canisters in a mechanistic-probabilistic way by considering a methodology that captures the onset of corrosion, crack initiation, and crack growth. Operating experience data is needed to validate the model as a whole. However, validation and calibrations on individual sub-models currently substitute this holistic validation gap, and improvements to address gaps in the parameterization of these sub-models are ongoing. A capability to halt crack growth as a way to simulate inspection and repairs is not currently implemented in the SNL approach, but an adaptation of EPRI's approach could be considered and added to consider all four stages. With proper parameterization for the sub-models that capture the four aforementioned stages, mechanistic-probabilistic modeling can inform the likelihood and timing of CISCC. The validated models will aid in risk-informing aging

management and inspection. Details of these models and corresponding parameters are discussed within this report.

TABLE OF CONTENTS

LIST OF TABLES

LIST OF FIGURES

ACRONYMS

AH	Absolute humidity
AMP	Aging management program
ASME	American Society of Mechanical Engineers
CFR	Code of Federal Regulations
CISCC	Chloride-induced stress corrosion cracking
CPL	Cumulative probability of leakage
CGR	Crack growth rate
CoC	Certificate of Compliance
DCPD	Direct current potential drop
DOE	Department of Energy
DCSS	Dry cask storage system
DSS	Dry storage system
EFPY	Effective full-power years
EPRI	Electric Power Research Institute
ISFSI	Independent spent fuel storage installations
POD	Probability of detection
NRC	Nuclear Regulatory Commission
NUREG	Nuclear Regulatory Report
RH	Relative humidity
RH_L	Limiting relative humidity
DRH	Deliquescent relative humidity
SEM-SE	Scanning electron microscope – Secondary electron
SCC	Stress corrosion cracking

SD	Storage duration
SNF	Spent nuclear fuel
SNL	Sandia National Laboratories
SRP	Standard Review Plan
SS	Stainless steel
Z_{ISFSI}	ISFSI ranking

1 INTRODUCTION

1.1 Dry Storage of Spent Nuclear Fuel

The United States currently has over 86,000 metric tons of commercial spent nuclear fuel (SNF) stored in dry storage systems (DSSs) at 78 independent spent fuel storage installations (ISFSIs) licensed by the U.S. Nuclear Regulatory Commission (NRC), an amount that grows by about 2,000 metric tons each year. Over 155,000 SNF assemblies have been loaded to date in over 3,500 DSSs across 34 states, at either operating or shutdown nuclear power plant sites, or away-from-reactor sites [1].

The NRC provides the regulatory framework for ISFSIs. Documentation for the regulatory framework can be primarily found in: 10 CFR Part 72 [2], NRC Regulatory Guides [3, 4], Nuclear Regulatory (NUREG) reports [5, 6, 7], and NUREG Staff Guidance. Initially the NRC's regulations in 10 CFR Part 72 limited the license term for a specifically licensed ISFSI or a storage system Certificate of Compliance (CoC) to 20 years. The NRC revised the regulations in 10 CFR Part 72 in 2011 to allow for longer initial periods of up to 40 years and renewals of specifically licensed ISFSI and stroage system CoCs for periods up to 40 years. Since then, a number of ISFSIs and storage system CoCs have been renewed for an additional 40 years of extended operation. The regulations in 10 CFR Part 72 require time-limited aging analyses and aging management programs (AMPs) as applicable to ensure that the safety functions of DSSs are maintained during the period of extended operation. AMPs include activities to manage issues associated with aging that could adversely affect systems, structures, and/or components important to safety. These activities include prevention, mitigation, condition monitoring, and performance monitoring of DSS components and subcomponents. The NRC has issued safety review guidance and technical reports to support the development of AMPs by applicants [8, 9, 10].

Over 90 percent of DSSs in the United States utilize canister-based designs deployed in either a vertical or horizontal configuration (see Figure 1-1) [1, 11]. In vertical systems, the canister sits upright within a steel-lined concrete overpack and is passively cooled by air entering through inlets at the bottom of the overpack and exiting through vents near the top. In horizontal systems, the welded canister rests on its side upon rails within a concrete vault. Air enters the overpack through a vent in the base, flows up and around the canister, and exits through vents on the roof.

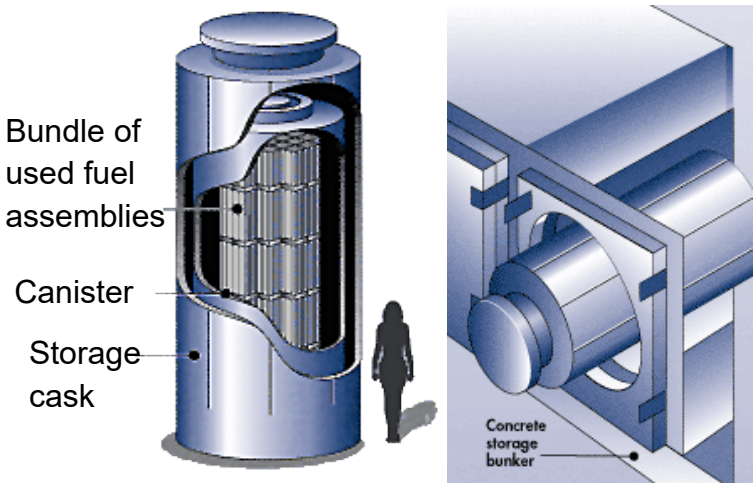

Figure 1-1. Typical dry cask storage system: Left is a vertical system, right is a horizontal system [11].

Most DSS canisters are fabricated from formed austenitic stainless-steel (SS), primarily 304 and 316 SS grades, which provides confinement of the SNF and serves as the primary barrier to ensure that radioactive material is not released to the atmosphere.

1.2 Relevance of Chloride-Induced Stress Corrosion Cracking

During operation of dry cask storage systems (DCSSs), the convective flow of exterior air entrains dust particulates with minerals and salts (and other deposits such as pollen, concrete dust, insects, etc), which accumulate on the canister external surface over time. These salts, particularly at near-marine environments, may be chloride-bearing, which can establish corrosive environments. These corrosive environments, in the presence of sufficient tensile stresses on the SS canister material may lead to chloride-induced stress corrosion cracking (CISCC). CISCC has been demonstrated to occur in the austentic SS grades used for DCSS canisters. Therefore, the potential for corrosion to occcur during extended periods of dry storage has led to significant efforts to ensure that adequate measures are taken so that its progression is limited and does not compromise the safety of DCSS [12].

The potential for CISCC in DSS canisters has been a subject of high priority research to confirm the regulatory technical basis in support of NRC-approved aging management programs. These efforts have been focused on enhancing the understanding of the susceptibility and progression of CISCC, as well as the necessary conditions for its occurrence.

Prior research has identified three conditions needed for CISCC to be initiated and sustained on the ouside surface of a canister. Figure 1-2 illustrates these three

conditions [12, 13]. First, the canister must be fabricated from material with metallurgical properties that make it susceptible to CISCC. The majority of canisters are fabricated from austenitic stainless steel (SS) of Type 304, while some designs are constructed with dual certified 304/304L and in some cases, 316 or 316L. It has been historically documented that these austenitic stainless-steel alloys can undergo CISCC [14, 15]. A second condition for CISCC to initiate is that an aggressive/corrosive environment must exist. Studies have shown that corrosive, chloride-rich salt aerosols can be deposited on canister surfaces from various sources including marine environments, road salts, and cooling towers [16, 17, 18, 19, 20]. Section 2.2 will discuss relevant chloride-containing salts for CISCC on DSS canisters, which are magnesium chloride ($MgCl_2$) and sodium chloride (NaCl). If deposited on a canister surface, the formation of a corrosive environment can be created as a result of salt deliquescence, which is a process where hygroscopic salt aerosols absorb water from the air in conditions of sufficient relative humidity (RH) to produce brines. Near-marine sites are considered to be especially at risk because of potentially high concentrations of chloride-rich sea-salt aerosols. The susceptibility of these materials to CISCC is dependent on the third criterion, which is that sufficient tensile stresses in a canister material must exist. The extent of residual tensile stresses on a canister surface varies due to variations in manufacturing and operations, including parameters such as degree of cold work and surface finish [21]. However, both modeling [22] and experimental measurements [23] have shown that through-wall tensile stresses are likely present in canister welds.

Research to fully understand the risk and timing of canister failure by CISCC is ongoing and evolving. For example, the Department of Energy (DOE) and Sandia National Laboratories (SNL) have been developing a probabilistically-based model for evaluating the potential of through-wall SCC. They have ongoing research efforts to reduce assumptions used for model prediction, particularly for sub-models that govern (1) brine evolution, both before and after initiation of corrosion, and (2) the corrosion processes of pitting, SCC crack initiation, and SCC crack growth. To address (1), DOE has been acquiring data to understand salt compositions and deposition rates at ISFSI sites. Similarly, DOE has also been investigating brine compositions over time for relevant canister surface environments. To address (2), DOE is focused on leveraging the data from (1) as well as measured SCC initiation/growth data to validate models for the statistical prediction of pitting and SCC initiation/growth for canister-relevant conditions [13].

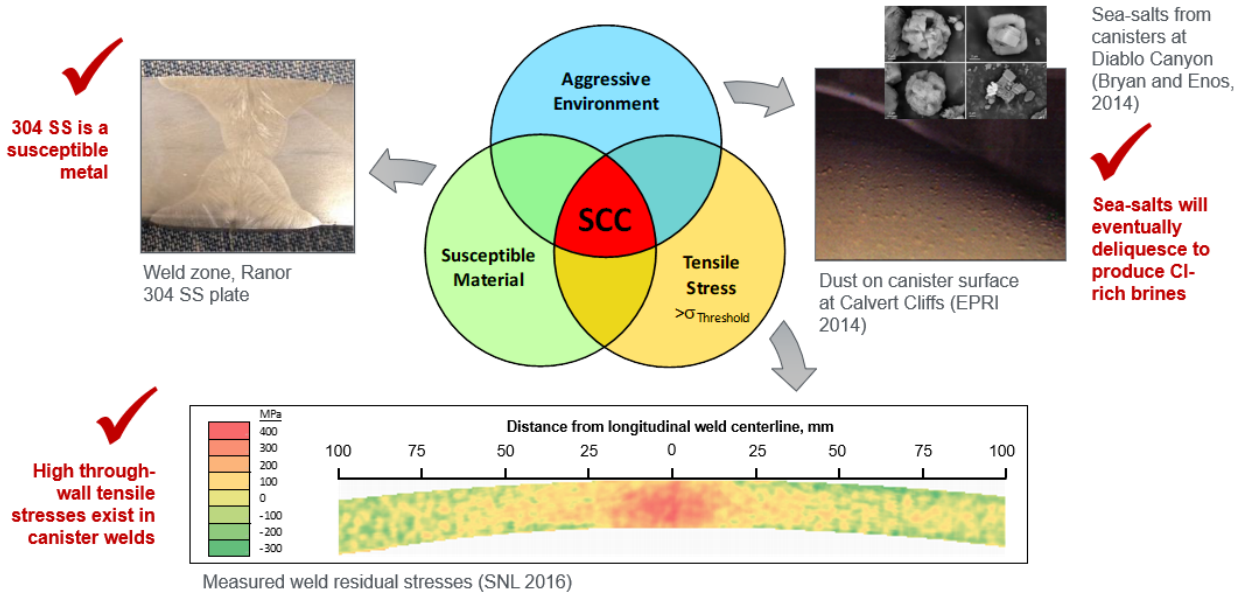

Figure 1-2. Criteria for CISCC to be initiated and sustained on a canister's surface [12].

1.3 Objectives of this Report

This report documents a preliminary scoping study that identifies and compiles the current state of knowledge on the susceptibility, crack initiation and growth, and consequences of CISCC. The purpose of this report is to support a technical basis in the assessment of the likelihood and timing of CISCC, which can support the NRC in efforts to risk-inform the generic requirements under the NRC-approved aging management programs and the inspection requirements in Code Case N-860 approved by the American Society of Mechanical Engineers (ASME) Boiler and Pressure Vessel Code.

2 PRELIMINARY ASSESSMENT OF STATE OF KNOWLEDGE ON CHLORIDE INDUCED STRESS CORROSION CRACKING

2.1 Overview of CISCC Mechanism

Austenitic stainless steel has exhibited susceptibility to stress corrosion cracking (SCC) when exposed to certain brines, particularly those brines rich in chloride [14]. The NRC has sponsored independent research, which confirmed that CISCC is an age-related (aging) mechanism that could potentially impact the performance of austenitic stainless steel canisters in DSSs [24, 25]. The NRC has continued to sponsor research to understand the factors impacting the susceptibility, progression and detection of aging effects related to CISCC, including localized corrosion and potential cracking.

During a canister's period of operation, the canister is passively cooled by convective air flow through the overpack vent openings. Over time, dust and salt deposits accumulate on the canister surfaces from entrained particulates in the air. Early in the storage period following placement of SNF inside a canister, temperatures may be too high on the canister surface to permit salt deliquescence (due to the inability of water to condense), and thus localized corrosion is very unlikely to occur. As the SNF cools, the RH at the canister surface will increase and salts to deliquesce if a critical relative humidity for the present salt is reached. The deliquescence can lead to a brine forming on the metal surface. Some of the deliquesced salts composing these brines may include aggressive species such as the previously mentioned chlorides, particularly for canisters near marine environments. These brines have been demonstrated to initiate localized corrosion and SCC when sufficient tensile stresses are present in the canister material. Understanding the propagation of a stress corrosion crack becomes of interest as it may compromise the confinement provided by a canister to SNF.

2.2 CISCC Progression

The susceptibility and progression of CISCC requires a systematic understanding and characterization of material, environmental, and operational parameters. Since 2014, DOE has been developing a probabilistic model to assess the potential and timing of through-wall cracking with CISCC. DOE's work has been primarily focused on acquiring data to improve the assumptions used in the sub-models within their CISCC probabilistic model. Their efforts have led to a methodology that provides insight to the physics occurring with CISCC progression [13, 21, 26, 27, 28, 29]. Figure 2-1 illustrates the CISCC progression considered by the DOE probabilistic model, where the various

sub-models are distinguished by the color-coded sequence. The figure illustrates how salt deposition is a precursor, after which a brine incubation period initiates the CISCC process prior to pits forming. That is, as a canister surface temperature cools and surface RH values increase, salts deposited on the canister during its storage period will deliquesce and form a brine on the canister surface, and the probabilistic model captures this. However, once a brine is present, manifestation of corrosion in the form of pits may be delayed for some time. The incubation period is thus defined by the interval of time occurring between two key points: (point A) when emplacement of the canister occurs, and (point B) when a corrosive brine developed from salt deliquescence allows pits to start forming on a canister surface. The full probabilistic model from DOE relies on mechanistically-based sub-models to capture individual processes and environmental parameters during canister storage to assess: (1) incubation and pit formation, (2) localized corrosion and pit growth, and (3) crack initiation (pit-to-crack transitions) and growth [12]. The subsections below discuss these different phases of CISCC progression.

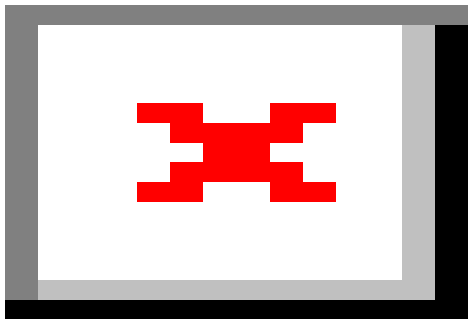

Figure 2-1. Schematic of parameters and sub-models in DOE's CISCC probabilistic model [12].

2.2.1 Deliquescence and Incubation

As previously mentioned, the incubation period for pitting refers to the interval of time required for a given canister surface location to cool to the point when the RH is sufficiently high for aerosolized and deposited salts to deliquesce and initiate corrosion. The incubation period is thus controlled by canister conditions (surface temperature) as well as by the environment (relative humidity and salt composition). As long as local RH on a canister surface is below a critical value (dependent on deposited salt composition), it is widely accepted that a brine is not expected to form and thus corrosion is unlikely to occur [21]. This theory lies on the premise that an external cathode is required to support corrosion of an anode (pit), and this external cathode can only be present when aqueous conditions exist on the metal surface of a canister [27] [30]. In the DOE probabilistic SCC model, the limiting RH value at which corrosion becomes possible is referred to as RH_L (also known as deliquescence RH), and therefore this convention is used in the remainder of this report. Whenever the local canister RH > RH_L, as determined by the canister surface temperature and environment relative humidity, aqueous conditions are considered to exist. In actual scenarios, aqueous conditions are reached and pits form after a period of time, but this length of time is taken to be negligible relative to representative storage times [15]. The time of pit initiation can thus be approximated by the point in time at which RH_L is first reached at a given location [31]. Environmental conditions can vary over time, however, and locations analyzed on a canister surface can go in and out of aqueous conditions. Thus, active corrosion can start/stop on a daily or seasonal basis, depending on the canister surface temperature, environment humidity, and how the brine/deposits on the canister surface change over time. In turn, the integrated time when RH > RH_L provides the total time when corrosion can actually occur, and this is referred to as the “time of wetness”. The size of the pits that form will depend on the canister surface environment. Over time, as the generation of decay heat slows (allowing the canister to cool) and as salt deposition from the environment increases, the pits can grow in size.

2.2.1.1 Salt-Dust and Brine Composition Effects

Once canisters are placed in their concrete overpack, dust and salt aerosols begin to deposit on the canister surface. DOE has been sponsoring research to understand the effects of the chemical and physical characteristics of the deposited dust and brines on CISCC susceptibility and progression. Understanding the composition of the deposited salts and dust is essential to understanding the risk of canister corrosion. Figure 2-2 shows the distribution of ISFSI sites across the U.S. Deposition of particles varies from

site to site and even spatially around a canister, but sampling and analysis of in-service canister surface dusts has documented the composition of particulate deposits at various locations that include: Calvert Cliffs, Maine Yankee, Hope Creek, and Diablo Canyon power plants [15, 17, 19]. These studies showed that dusts mostly contain detrital mineral grains, mostly quartz and aluminosilicate minerals such as feldspars and clays. Salts at these locations consisted of a mixture of marine salts (Na^{+}, Cl^{-}, Mg^{+2}, SO_4^{-2}) and a composition referred to as a "continental component" (Ca^{+2}, K^{+}, (NH_4^{+}), NO_3^{-}, SO_4^{-2}), which are constituents that are derived from land-use or other anthropogenic processes [15, 17, 19].

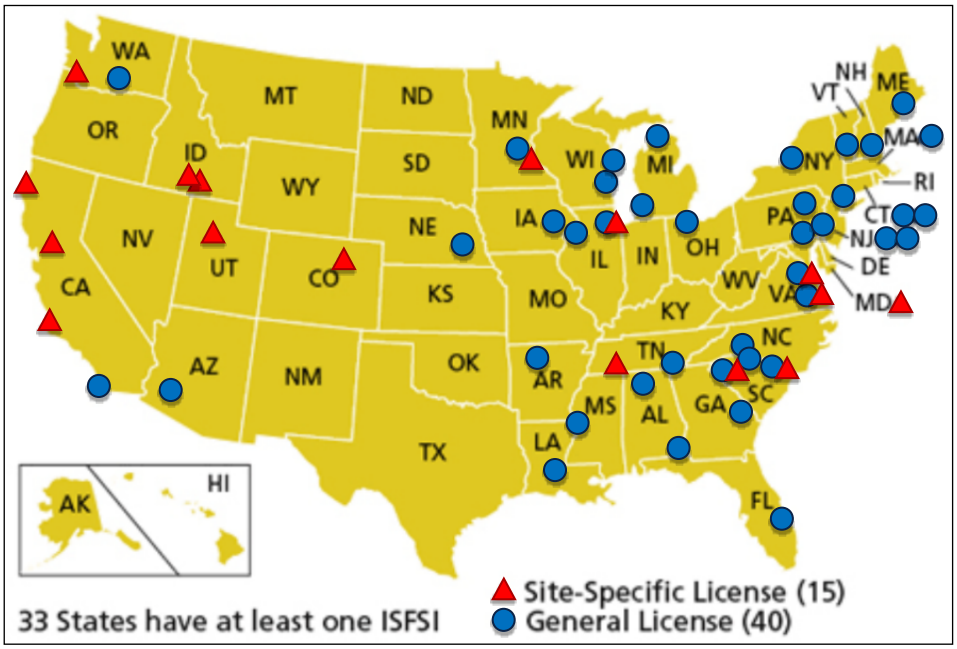

Figure 2-2. ISFSI locations across the U.S [32].

The chemical composition of the salts deposited on the canister surface influences both the RH at which deliquescence occurs and how corrosiveness a formed brine can be. Various studies have been carried out to understand the evolution of brines on canister surfaces. In the 2022 work of Bryan *et al.*, thermodynamic modeling of seawater evaporation was performed to study the compositional evolution of brines that are formed by the deliquescence of sea salt aerosols under a range of relative humidity values at 25 °C [32]. Figure 2-3 illustrates the composition of these sea salts at a range of relative humidity values. Bryan *et al.* explain the evolution in the following manner

[32]: At higher relative humidity as seawater evaporates at 25 °C, the initial phases to precipitate are relatively low solubility calcium carbonate, magnesium sulfate, and calcium sulfate, all precipitating at greater than 90% RH. As evaporation continues, the hydrated sulfate phases redissolve and reprecipitate as less hydrated equivalents. The brine is dominantly Na^+ and Cl^- at higher RH until halite precipitates at ~74% RH. With continued evaporation, potassium-containing (K-containing) quaternary sulfates (polyhalite) and ternary chlorides (carnallite) precipitate, depleting K from the remaining brine. The brine evolves towards an increasingly magnesium-rich composition and at this point, the brine is almost entirely magnesium chloride until bischofite ($MgCl_2$:$6H_2O$) precipitates at 36% RH. These values are consistent with prior work observed in literature as compiled by SNL [15].

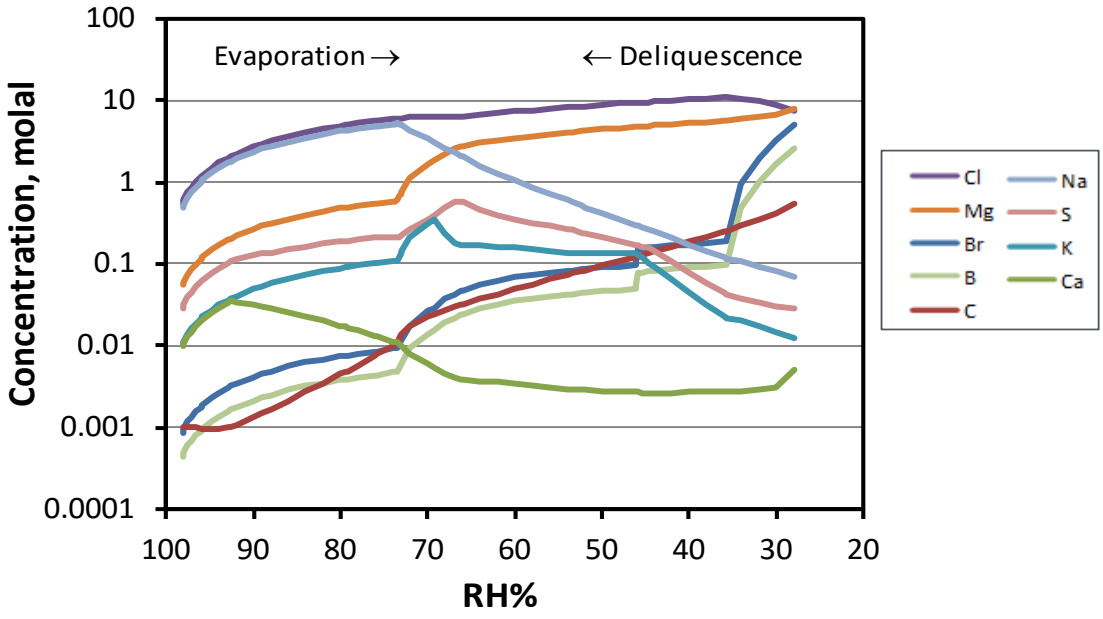

Figure 2-3. Deliquescence of sea salts at 25 °C [32].

2.2.1.2 Canister Thermal Environment

A canister surface environment is initially at very low RH as the canister surface temperatures are hot after emplacement of the SNF. Therefore, understanding the evolution of the brine as discussed above has multiple implications. As a canister surface with deposited sea salts cools and local RH rises over time in spots around the

canister, the deliquescent brine would experience a compositional transition analogous to going from right to left in Figure 2-3. That is, it's the highly deliquescent bischofite ($MgCl_2$:$6H_2O$) that is believed to control the initial deliquescence behavior of sea salts, while sodium chloride is dominant much later, when cooler temps produce higher RH around the canister.

Using typical annual weather conditions at Calvert Cliffs, MD and a horizontal canister thermal model based on Transnuclear (now Orano) NUHOMS systems (at Calvert Cliffs), SNL has modeled the potential thermal evolution of the surface environment of a horizontal canister over a period of almost 300 years [15, 33]. The model was run at different heat loads to simulate decay heat at different points in time after placement in storage. These heat loads with corresponding times are captured in Table 2-1. Running CFD models with these loads and the identified weather conditions resolved to temperature maps as shown in Figure 2-4. Using the CFD models, 35 key points on the canister surface were chosen as shown in Figure 2-5, where Figure 2-6 shows the thermal evolution of these points over the 292 years described in Table 2-1. Knowing these canister surface temperatures, the RH on a canister surface can be calculated for a given absolute humidity (AH) of the air entering the overpack by using an equation of state for water to correct for the change in temperature [15, 34]. If a conservative scenario is assumed with a cool ambient temperature at 15.5 °C, saturated air (RH=100%) would consist of an AH of 13.3 g/m^3. The CFD calculations performed by SNL thus indicated that, when considering NaCl, conditions for deliquescence (RH > 75%) would not be reached when considering the simulated 292 years with the given input parameters (see Figure 2-7). For $MgCl_2$, on the other hand, the studies showed that sea-salt brines could be exposed to relative humidity conditions that would result in development of $MgCl_2$ in less than 20 years at the coolest locations on the canister surface (RH >35%).

Table 2-1. Heat Loads and Corresponding Times for Horizontal CFD Model [15, 33]

Heat Load [kW]	Corresponding Elapsed Time [years]
24 kW	0
20 kW	2
15 kW	7

10 kW	12
8 kW	27
6 kW	42
4 kW	92
2 kW	292

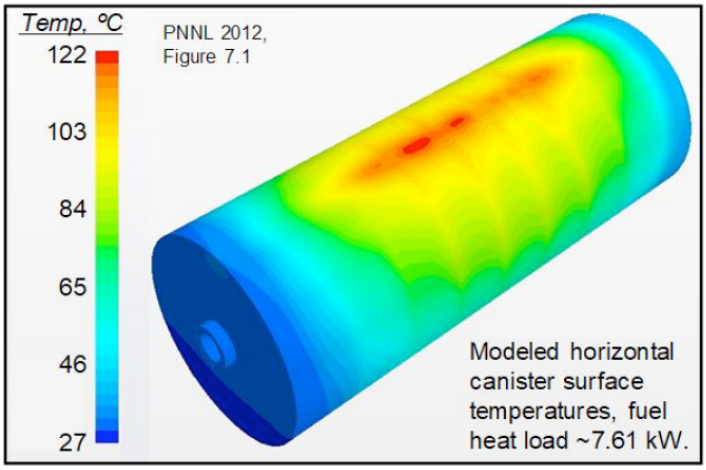

Figure 2-4. Predicted temperatures on a canister surface for the Calvert Cliffs NUHOMS model at a heat load of 7.61 kW [15, 33].

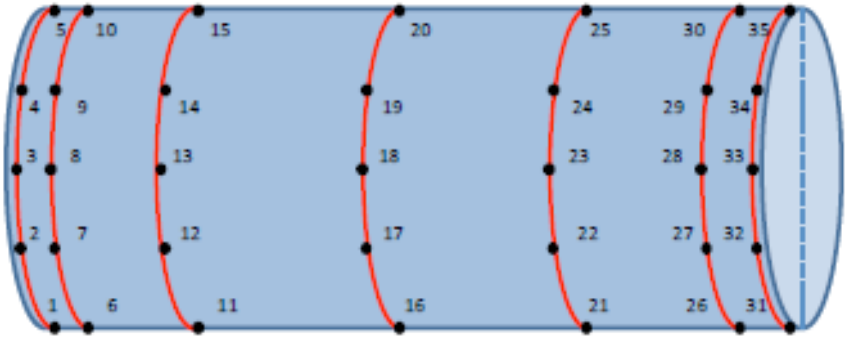

Figure 2-5. 35 key points chosen on Calvert Cliffs NUHOMS model [15, 33].

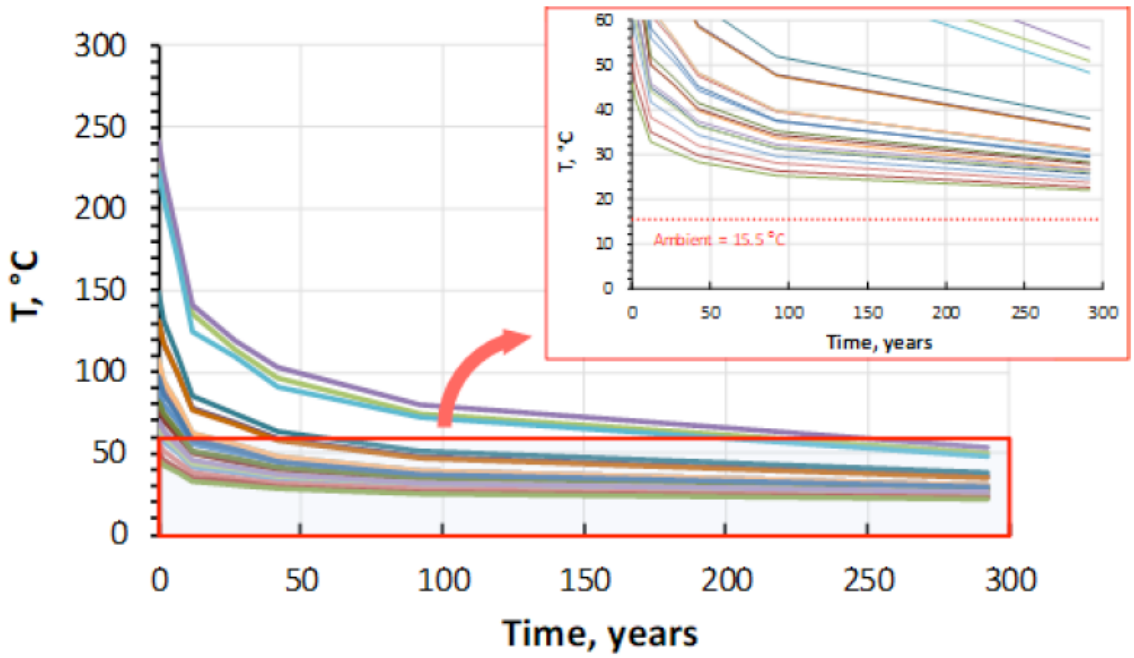

Figure 2-6. Predicted evolution of canister surface temperatures at 35 key points chosen on Calvert Cliffs NUHOMS model assuming an ambient air temperature of 15.5 °C [15, 33].

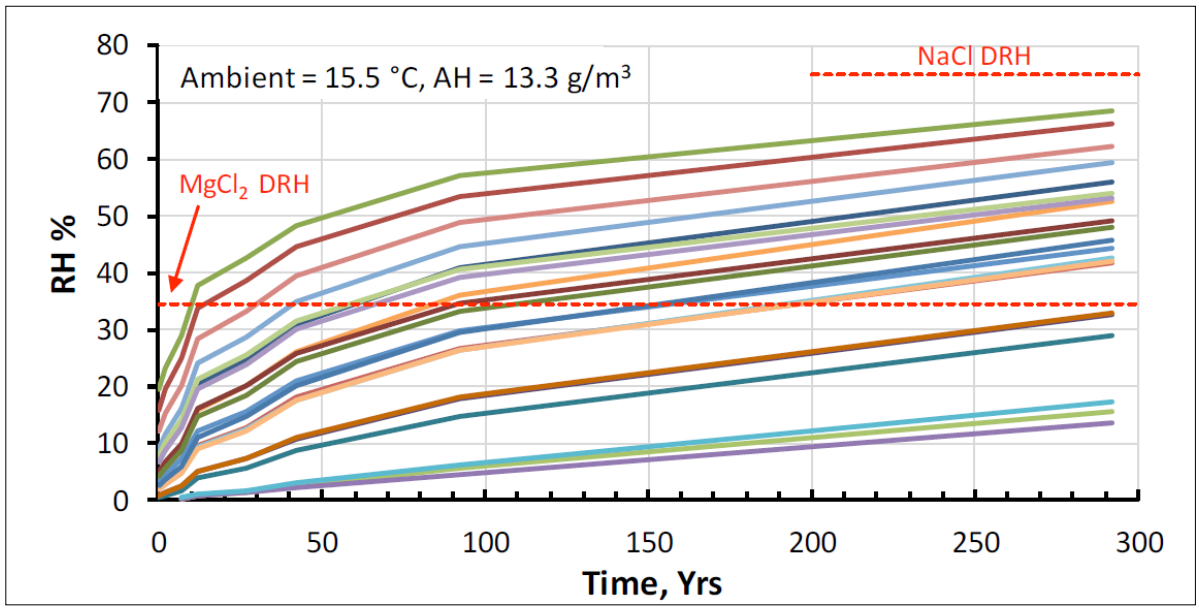

Figure 2-7. Predicted RH on Calvert Cliffs NUHOMS thermal model for Saturated air at 15.5°C, where DRH = Deliquescent RH [15, 33].

2.2.1.3 Diurnal-Cycle Effects

Canister temperatures are hottest immediately after emplacement and decrease as the SNF heat decays over time. Diurnal-cycling effects are expected on a canister surface due to the fluctuating environmental conditions on a DCSS. Specifically, for a canister within its overpack, air will cool its surface as it flows from ambient conditions through inlet vents at the base and then goes up and around the canister. With ambient air being cooler than canister surface temperatures, the air heats up as it flows from the base up and around the canister. This pathway for the airflow results with canister surface temperatures coolest at the base. In realistic scenarios, the cooling air temperature at storage sites naturally varies throughout the day while AH tends to stay relatively constant, but both may change seasonally. Relative humidity, however, is a function of two properties: (1) the AH of the cooling air entering the overpack and (2) the canister surface temperature. As discussed in the previous subsection, at any given point, this canister surface temperature is a function of the heat load and the temperature of the ambient air flowing through the overpack. Despite a robust canister thermal mass, the passive cooling systems do cause rapid changes in canister surface temperatures as changes in airflow temperature occur. Thus, due to fluctuating ambient temperatures, decreasing thermal load from the SNF, and spatial distribution of temperature on a canister, diurnal cycles occur in the local RH as well. These

fluctuations in turn can significantly affect the composition and amount of deliquesced brine on a daily basis. According to a study from DOE in 2020, under the right conditions, daily temperature changes can cause the RH at a canister surface to fluctuate above and below the limiting deliquescence RH for the deposited salts [18]. As a result, these fluctuations in ambient conditions may cause the brines to dry out and re-wet on a daily basis. These cyclic changes in temperature and RH can consequently result in more aggressive environments than constant conditions [35].

SNL has ongoing efforts to evaluate the effects of cyclical changes and periodic dry-out. The goal of these tasks is to utilize real ISFSI site-specific weather data to develop a realistic model for coupled diurnal variations in temperature and RH on a heated canister surface. SNL's objectives are to evaluate the cyclical changes to CISCC initiation [36, 37]. SNL identified that prior works did not cycle canister temperature and RH in ways that captured their natural environment [36]. To improve upon these works, SNL focused on cycling temperature and RH conditions in a way that temperature and RH are inversely correlated with minimal adjustments to AH. SNL's initial goal was to identify conditions for sea-salts that can result in daily dry-out and re-deliquescence: where the RH repeatedly fluctuates above and below the deliquescence RH for sea-salts. To identify these realistic diurnal cycles for temperature and RH, SNL examined weather data sets representative of three different ISFSIs: Arkansas Nuclear 1 in west-central Arkansas; San Onofre on the Pacific coast between Los Angeles and San Diego, California; and Turkey Point on the Atlantic coast just south of Miami, Florida. Of the three different locations analyzed for daily cycling over the bischofite ($MgCl_2{:}6H_2O$) deliquescence RH, the Arkansas Nuclear 1 cycle fluctuated with the largest range of RH values due to large daily temperature swings Figure 2-8 shows the measured data on the top left at ambient conditions for a full year, while the right column shows measured data focused on the summer interval. The middle and bottom rows in Figure 2-8 show the RH response if AH is maintained as measured but with increased temperatures (+10 °C for middle row, and +20 °C for bottom row). Figure 2-9 zooms in on seven summer days as an example and shows how the case with an added 10 °C diurnally crosses the deliquescence RH for $MgCl_2$ previously discussed (RH ~36%) . Furthermore, in this exercise shown in Figure 2-9, SNL showed how the diurnal RH data could be replicated with a best-fit curve if an average AH was maintained. The ability to reproduce the diurnal cycle that fluctuates around the deliquescent RH for $MgCl_2$ with this simplified approach is significant for future investigations. Specifically, this simplified reproduction can be helpful for future experiments where diurnal temperature and RH need to be produced for a representative environment.

This site exhibited a high average AH, which means that a deliquescence RH can be encountered at higher temperatures and thus initiate corrosion earlier in the storage

process. The large daily temperature swings, when paired with a relatively stable AH, increase the probability of dry-out and re-wetting. The Arkansas Nuclear 1 cycle was thus determined as the most conservative cycle and recommended for use in any future work attempting to simulate conservative diurnal cycles [15].

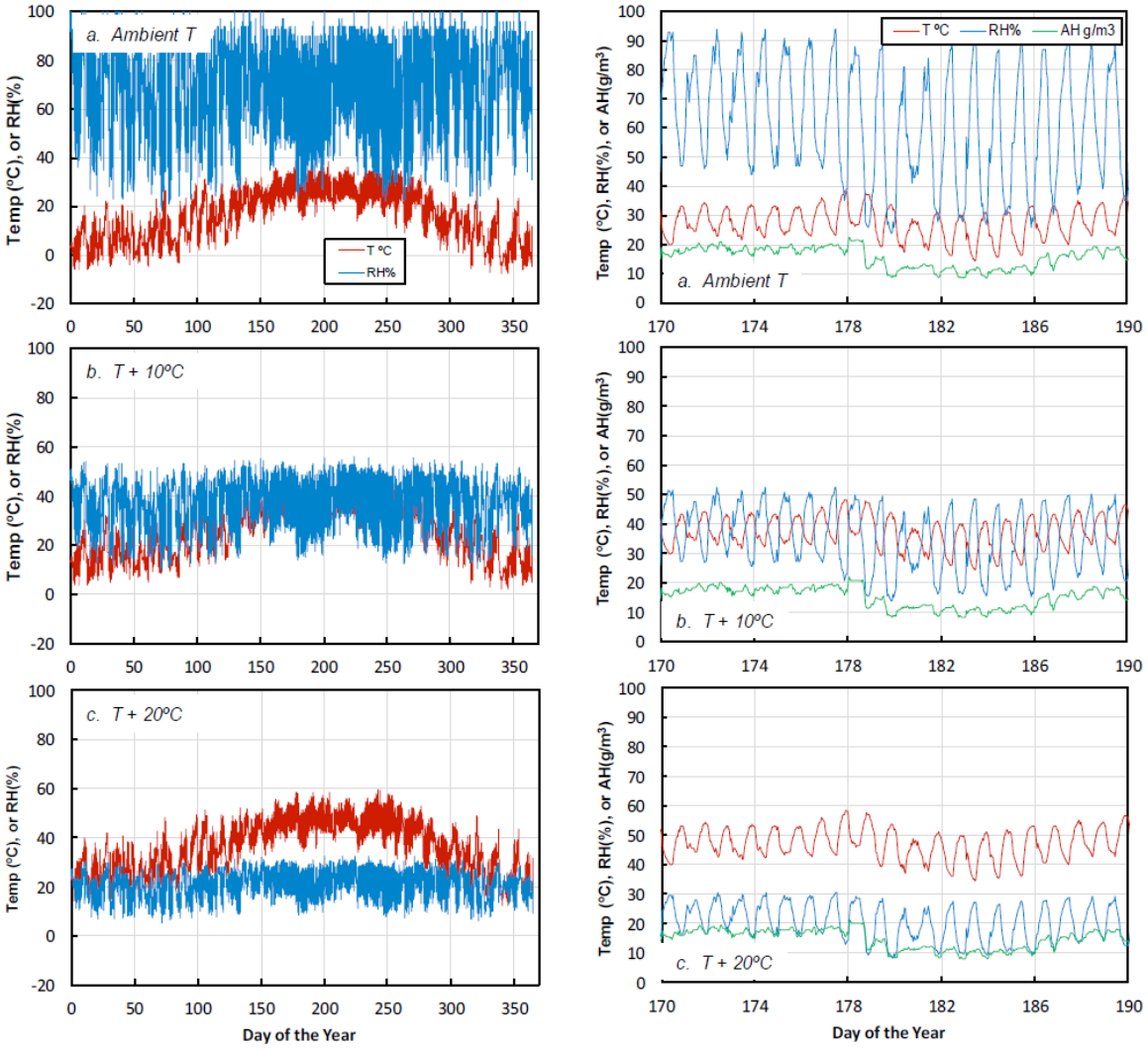

Figure 2-8. Temperature and RH variations at Arkansas Nuclear 1 site. Yearly data on the left, and summer interval on the right. Top -- ambient T; Middle -- ambient T+10 °C; Bottom -- ambient T+20 °C [15].

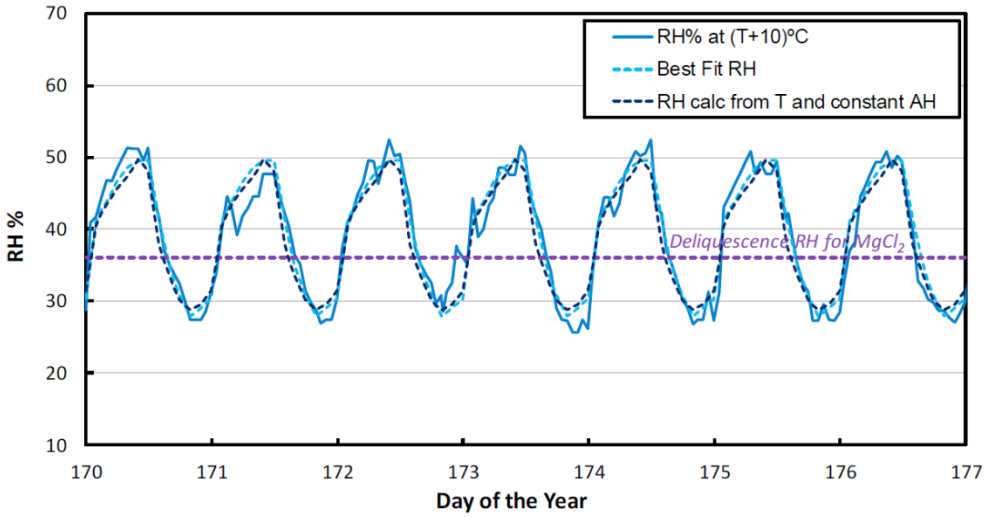

Figure 2-9. Arkansas Nuclear 1: Temperature-adjusted weather data with best-fit diurnal cycle that crosses bischofite deliquescent RH. Best-fit diurnal cycle with simplified AH is also shown.

2.2.2 Pit Initiation and Pit Growth

Prior work has demonstrated that pitting initiation and pit growth rates are strongly correlated with environmental factors such as canister temperature, relative humidity, and salt load, but also by canister material properties, including composition, surface finish, microstructure, and stress level. Experimental work from Weirich *et al.* and Srinivasan *et al.* has shown that pit morphology was highly dependent on local RH [38, 39]. For 304 stainless steels exposed to sea salt microparticles, both studies saw that as exposure RH changed, various characteristics of the brine development changed with potential to influence pitting: surface water layer thickness, brine morphology, formation of solid precipitates, conductivity, and brine concentrations.

In their experimental work performed in 2019, Weirich *et al.* studied the evolution of 304 stainless steel when exposed to representative corrosive environments. They studied how coarse-ground 304 stainless steel evolved when samples with deposited sea-salt particles were exposed to 40% and 76% RH atmospheric environments at 35 °C. Comparing the results of developed pits revealed that the samples experienced significantly different morphology after one year: Total corrosion damage was higher at 40% RH exposure compared to the 76% RH exposure. Hemispherical and ellipsoidal pits with crystallographic surfaces were formed at 76% RH. Salt particles exposed to the 40% RH resulted in brines that created rough, irregularly-shaped pits where cracks

were observed to spread from the pits that formed in these exposures. Scanning electron microscope (SEM) images captured using a secondary electron (SE) mode for the 40% RH atmospheric exposure can be seen in Figure 2-10. SEM-SE images of pits resulting from the 76% RH atmospheric exposure can be seen in Figure 2-11. The differences in pit morphology and cracking in the 40% RH case are apparent when comparing these two figures.

In the same work, Weirich *et al.* also studied stainless steel samples exposed to fully-immersed brine solutions with compositions that resembled brines which develop for sea-salts exposed to 40% and 76% RH, respectively. These studies showed milder damage than the atmospheric tests (see Figure 2-12), but within the fully-immersed tests, the 40% RH-equivalent brines still showed more damage. The pit distribution was also more dense and uniformly distributed for the lower RH when compared to the higher RH on the surface. Investigations are underway to understand why cracking was observed in the 40% RH-equivalent brine exposure and not in the 76% RH-equivalent exposure [13, 38, 39], but the 40% RH exposure generally showed that aggressive corrosive environments can develop during early stages of storage if $MgCl_2$ is present. In 2021, Srinivasan *et al.* performed similar studies to that of Weirich *et al* [38, 39], but these investigations studied the evolution of pits for prolonged exposures. *S*tainless steel specimens were exposed to the same environments as the Weirich *et al.* study for periods from 1 week up to 2 years, and pits that developed were characterized using profilometry, electron microscopy, and X-ray microtomography. Overall, the behavior observed by Srinivasan *et al.* was consistent with the observations of Weirich *et al.*, except that pit densities and volume appeared to approach plateaus at long exposure times, especially for the 40% RH exposure.

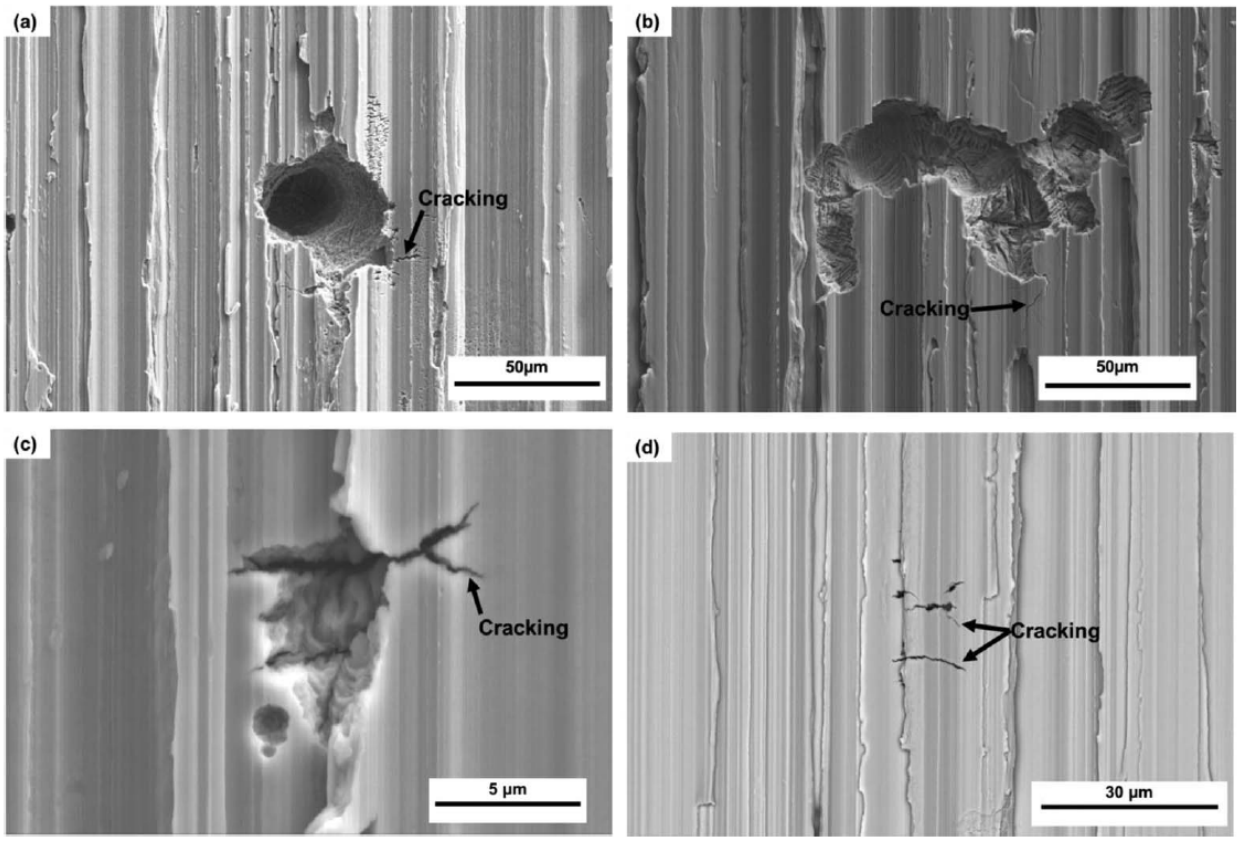

Figure 2-10. SEM-SE images of pits resulting from intact SS304 at 40% RH atmospheric exposure showing: (a) large individual pit, (b) coalesced pit, (c) small pit with associated crack, and (d) crack not associated with a visible pit [38].

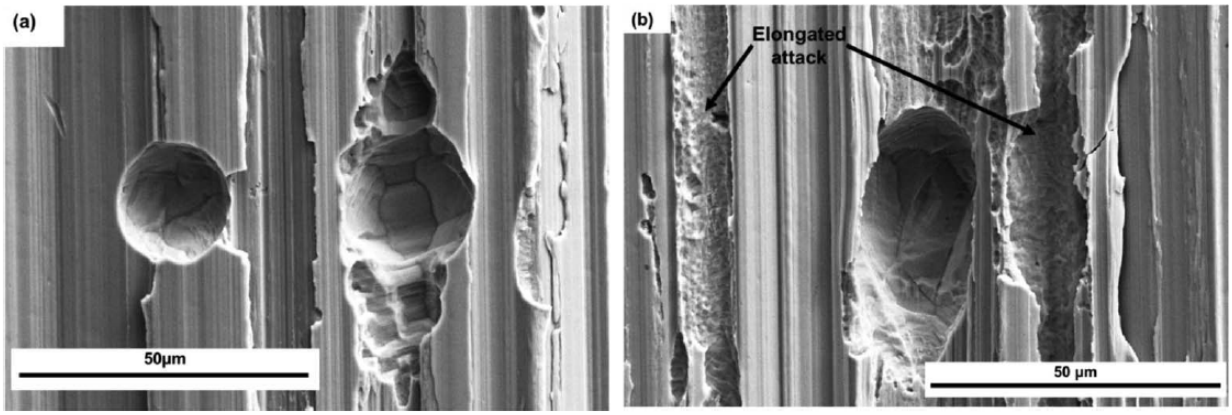

Figure 2-11. SEM-SE images of pits resulting from the 76% RH atmospheric exposure showing (a) ellipsoidal pits, and (b) shallow elongated pits adjacent to an ellipsoidal pit [38].

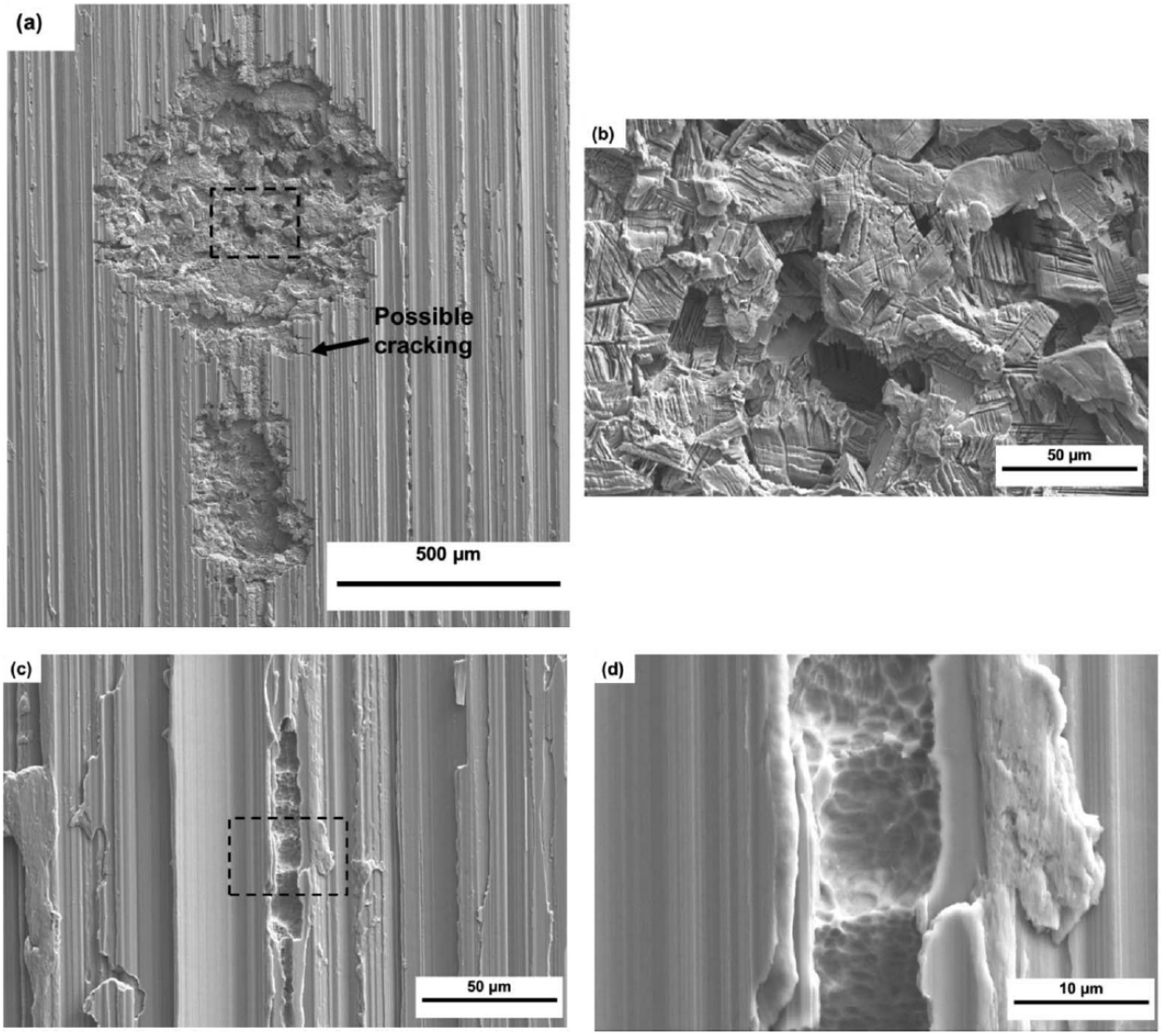

Figure 2-12: SEM-SE images of pitting for SS304 resulting from full-immersion tests corresponding to 40% RH-equivalent ((a) and (b)) and 76% RH ((c) and (d)). Note: images (b) and (d) are the magnifications outlined by the dashed rectangles in (a) and (c), respectively [39].

2.2.2.1 Maximum Pit Size Model

Pits formed on canister surfaces generate aggressive chemistry and act as local stress concentrators, and they are therefore determining factors that influence crack initiation as observed in the previous subsection. Understanding pit morphology on canister surfaces is thus a critical step for understanding crack formation. The differences in morphology described in the previous subsection can be partially explained through understanding solution chemistry. Given the aforementioned dynamics, various approaches exist to properly capturing the chemistry and effects of pits on canister surfaces. The work of Chen and Kelly targeted the modeling of maximum pit sizes based on environmental and surface characteristics, and DOE uses a version of this maximum pit size model in their probabilistic assessment of SCC [40, 41, 42]. With the Chen and Kelly approach, once a pre-defined critical RH is reached, a maximum pit size model is used to evaluate the deepest pit that can develop on a surface as a function of several environmental parameters. This approach assumes that pit nucleation is not a limiting factor in pit formation and that pits rather nucleate instantaneously once an environment's RH is greater than a pre-defined threshold. Over time, as a canister cools and salt deposition increases, the maximum pit size increases, and the Chen and Kelly approach reflects that. In this model, in order for a pit to undergo stable growth, the cathodic current (I_c) available to support pit growth must exceed the anodic current (I_{pit}) demand for the pit stability. The maximum pit size can then be calculated by determining the maximum cathode current as a function of pit size and comparing it to the predicted anodic current demand as a function of pit size. The ability of the cathode to supply current to the anode is controlled by the thickness and ionic strength of a brine layer on the metal surface. The Chen and Kelly model assumes a hemispherical pit with a radius r_{pit} for simplification purposes [40, 41]. A pit stability criterion expressed as I_{pit}/r_{pit} for a hemisphere then determines the point from which a pit can grow. If a value is identified for the pit stability criterion, I_{pit} can be calculated as a function of the pit radius. In the Chen and Kelly model, the maximum cathodic current, $I_{c,max}$ is expressed as:

$$\ln I_{c,max} = \left[\frac{4\pi\kappa t\Delta E_{max}}{I_{c,max}} + \ln\left(\pi e r_a^2 i_{eq}\right)\right], \qquad (2\text{-}1)$$

Where:

- κ is the brine conductivity
- t is the brine thickness
- $\Delta E_{max} = E_L - E_{rp}$ is the potential drop from the pit edge to the outer cathode edge
- e is Euler's number
- r_a is the anode (pit) radius
- i_{eq} is the maximum equivalent current density for the cathode.

Derivation of the values for these parameters is beyond the scope of this report but it is described in related papers published by the authors [40, 41, 42, 43, 44, 45] . Several of the parameters vary with the environmental conditions on the canister surface (temperature, RH, and salt load), including the brine conductivity, brine thickness, and the maximum equivalent current density for the cathode. Utilizing this model and assuming a salt deposition rate, a maximum pit size can be calculated at a given location on a canister surface at each time step considered in a probabilistic model such as DOE's. If the maximum cathodic current is calculated from Equation (2-1) and the anodic current is calculated from the pit stability criterion, the maximum possible pit size corresponds to the size at which the two values equate, as shown in the example plotted in Figure 2-13.

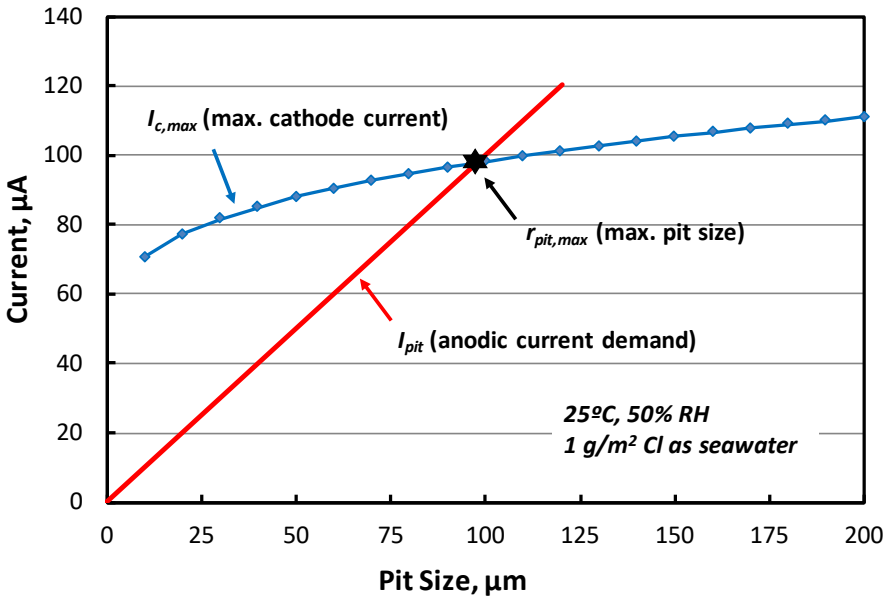

Figure 2-13: Chen and Kelly approach for estimating the maximum pit size [42, 45].

2.2.3 Pit-to-Crack Transition Model

Discussions from sections above show how both the environment and material properties play a role in the resultant corrosion damage on stainless steel coupons. Pits eventually grow large enough to serve as nucleation sites for stress-driven cracks. SCC cracks initiate from corrosion pits in a stochastic process, and the likelihood of SCC initiation increases as the pit deepens [31]. Understanding pit-to-crack transitions has been attempted through modeling. Existing models relate pit depth to crack initiation through a calculated crack tip stress intensity factor. A sample implementation is in the SNL SCC probabilistic model, where a pit-to-crack transition sub-model is used to evaluate when a crack initiates. In this approach, once a limiting RH (RH_L) value for corrosion is reached and pits have formed, stress corrosion cracks can initiate from the assumed hemispherical pits if a pit reaches an empirically-determined threshold. This threshold value is calculated using the Kondo criterion, where larger pits increase the probability of stress corrosion crack formation [46, 47]. Conditions that produce thicker brine layers, such as heavy salt loads or moderate increases in RH, increase the size of possible pits that can form, and thus these factors also increase the likelihood of SCC initiation. With the Kondo approach, a crack tip stress intensity factor (K) is calculated for a crack of equivalent depth as a known pit (obtained from maximum pit-size model) using data from tensile stress profiles. Stress distribution influences the stress intensity factor, and in areas where higher tensile stresses pre-exist, K will increase more rapidly with depth, allowing pits to initiate SCC more easily. This sub-model matches some observations previously observed in experimental studies [37]. A crack will initiate if the calculated K exceeds a critical K for SCC, which is referred to as K_{ISCC}. As values for K_{ISCC} vary in the literature, the SNL SCC model takes a probabilistic approach and samples once per realization from a range of literature values. Although this approach is simplified, this combination of the maximum pit-size model and the described pit-to-crack transition model provide insights into the process of SCC crack initiation.

2.2.4 Crack Propagation

Once cracks initiate, they can propagation varies depending on environmental factors. Spent nuclear fuel canisters are commonly fabricated from either a 304 or 316 stainless steel alloy, and there is currently limited data on crack growth rates (CGR) for these

alloys [13]. A literature review compiled by Bryan & Enos illustrated a temperature dependency for CGR, as shown from their work in Figure 2-14 [48].

Bryan led an effort in 2020 to investigate how crack initiation/growth are influenced by environmental conditions at ISFSIs for SNF canisters, specifically brine composition and temperature conditions. CGR was measured using high fidelity direct current potential drop (DCPD) systems in a temperature-controlled solution ranging from 20 to 75 °C with CO_2-scrubbed air [15, 48]. However, these studies showed minimal dependence of CGR on brine composition, and a dependence on temperature was not obvious [15, 48]. SNL is currently working on new and more comprehensive measurements with an upgraded DCPD system that includes four servomechanical load frames to enable in-situ measurements of crack length over long periods of time [13]. This work is ongoing with a proof-of-concept to establish the test setup, where CGRs will be tested on SS304 and SS316 samples [15].

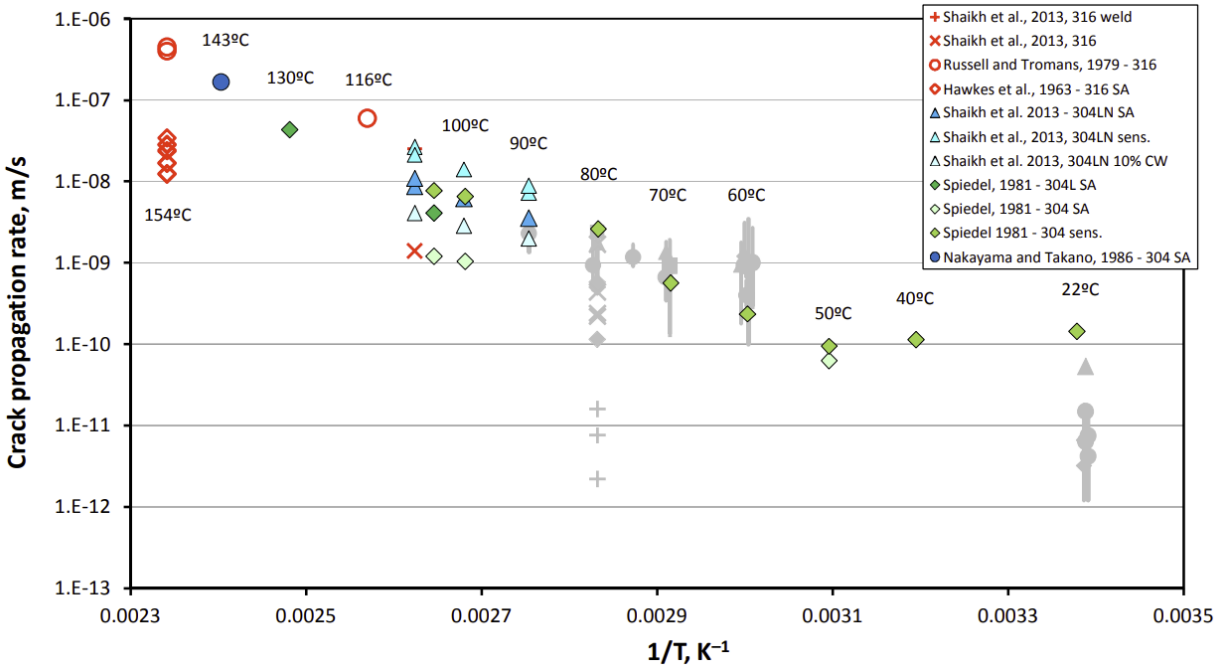

Figure 2-14. Crack propagation rate data collected under immersed conditions for chloride-rich brines [48].

Due to the limited data on crack propagation, modeling of CGRs has been previously performed with probabilistic-mechanistic approaches [49]. A common model used is that of Wu and Modarres, which assumes a power-law dependence for the stress intensity factor and an Arrhenius relationship for the temperature dependence [29, 46, 49]. The CGR can thus be defined by

$$\frac{dx_{crack}}{dt} = \dot{x} = \alpha \cdot exp\left[-\frac{Q}{R}\left(\frac{1}{T} - \frac{1}{T_{ref}}\right)\right] \cdot (K - K_{th})^{\beta} \qquad (2\text{-}2)$$

where:

- $\frac{dx_{crack}}{dt}$ is the crack growth rate (m/s), also denoted $\dot{x}$,
- T is the temperature (K) of interest,
- α is the crack growth amplitude (crack growth rate at reference temperature),
- β is the stress intensity factor exponent,
- Q is the activation energy (J/mol) for crack growth,
- R is the universal gas constant (8.314 J mol^{-1} K^{-1}),
- T_{ref} is a reference temperature (K) at which α was derived ($15.55℃ = 288.7\ K$ was used in this study),
- K is the crack tip stress intensity factor, and
- K_{th} is the threshold stress intensity factor for SCC.

In the SNL implementation, the uncertainty in crack growth amplitude and stress intensity factor exponent are captured using uncertainty distributions and are determined by a combination of assumptions and calibration to experimental data [26].

3 RISK SEQUENCE

A review was performed on EPRI's model to assess the probability of a crack penetrating through-wall in a SNF canister. A summary of that review is documented here, not as our original work [50]. EPRI's assessment is implemented in a probabilistic fashion, using a Monte Carlo approach. This approach allows uncertainty to be captured, whether that's due to inherent randomness in some of the stochastic processes, or whether it's due to an incomplete understanding of modeled processes. Within the Monte Carlo approach, there are deterministic models which take inputs that are sampled from statistical distributions. These distributions aim to capture the uncertainty of the input parameters. The Monte Carlo analysis is thus performed by executing a pre-defined number of deterministic calculations for each set of randomly sampled input values from corresponding distributions, where each run/iteration is referred to as a realization. As the number of realizations are increased using such an approach, aggregated values from the realization results (such as the mean) will tend to converge and yield the result of the probabilistic analysis.

In the analysis reviewed here, each realization models a chosen number of canisters that are each discretized into a number of potential flaw initiation sites (defined as an input parameter to the model). Each discretized flaw position has the potential for one crack that can grow to penetrate the canister wall. Interaction between flaw positions for cracks (coalescence) is not considered/modeled. The full Monte Carlo analysis duration is controlled by three main parameters: Duration of analysis for each realization, incremental timestep, and total number of realizations (where each realization models a pre-defined set of canisters over the chosen time frame).

An overview of the probabilistic model is captured by Figure 3-1. The general model inputs are: number of realizations, number of canisters per realization, number of flaw positions per canister, simulation time step, and total time period considered. The model can be broken up into three main modules that respectively cover flaw initiation, crack growth, and inspections on the simulated canisters. The flaw initiation model focuses on stochastically initiating cracks at considered flaw positions based on canister properties, ISFSI location, and environmental factors at the ISFSI location. The crack growth model focuses on probabilistically modeling how fast the initiated cracks/flaws grow. The inspection model focuses on simulating random inspections to determining whether initiated cracks can be identified and repaired before becoming through-wall. These three main models are discussed in detail in the subsections below. It should be noted that the approach discussed here can be applied to vertical or horizontal configurations, but the orientation-dependent parameters summarized here are only for horizontal canisters (for vertical canister parameters, the reader is referred to EPRI’s full work [50]).

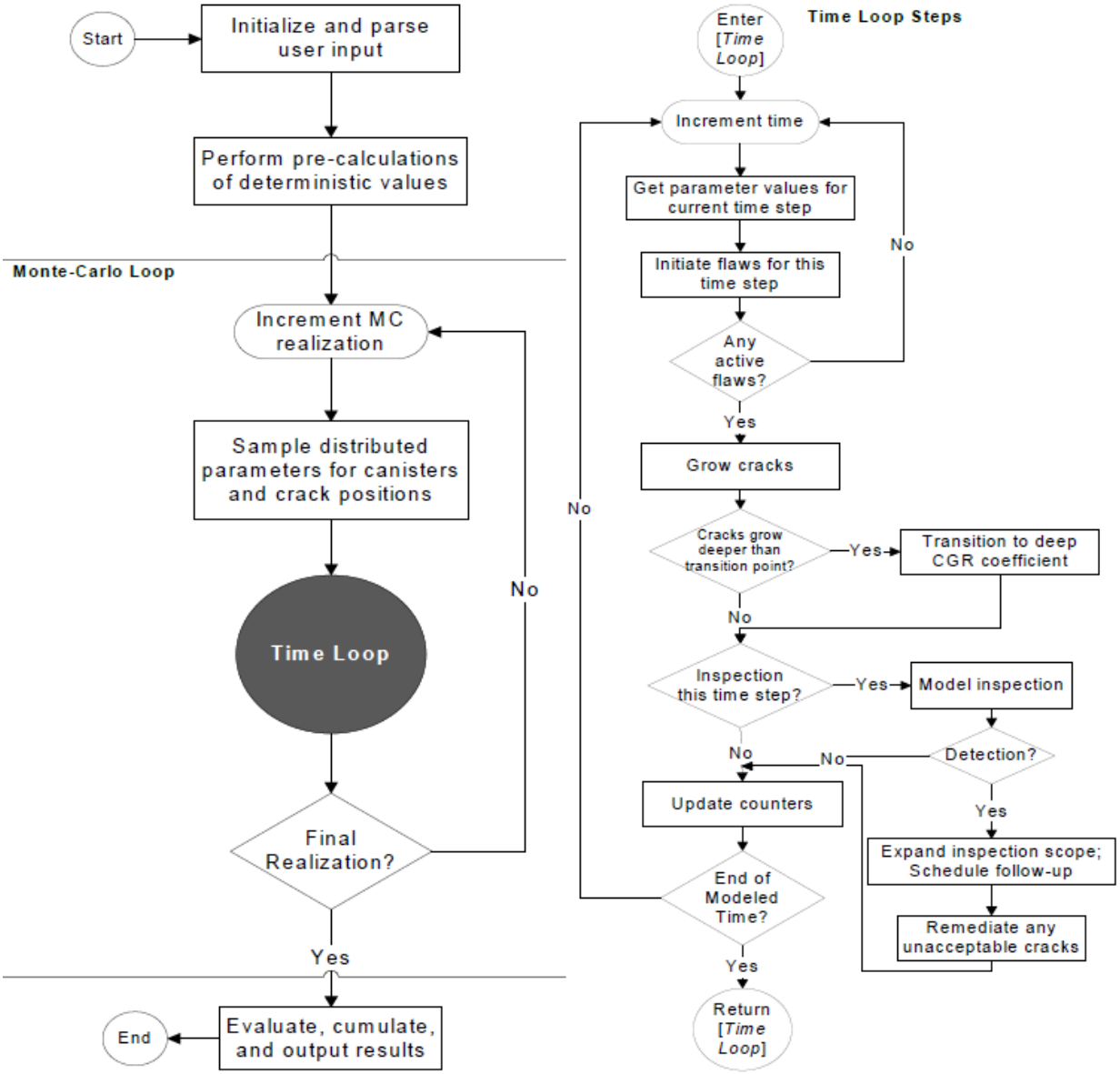

Figure 3-1. Flow chart for probabilistic model [50].

3.1 Flaw Initiation

Flaw initiations on a canister are performed using an initiation probability that is dependent on the canister's susceptibility. Susceptibility of a canister at a given time was assessed in this work using the ranking criteria established by EPRI in their 2015 *Susceptibility Assessment Criteria for CISCC of Welded Stainless Steel Canisters for Dry Cask Storage Systems* report [51]. Initiation is modeled by calculating an initiation probability for a canister while considering an initiation probability threshold for each

canister flaw position from a distribution. The initiation probability starts at zero when the canister enters service and asymptotically approaches one as time marches. The initiation probability for each canister increases on an annual basis based on a known ISFSI rank (Z_{ISFSI}) and storage duration.

3.1.1 Determination of Susceptibility

A susceptibility rank is assigned to each modeled canister based on the approach described in EPRI's 2015 work [20, 47]. Three main components sum up a canister's ranking: Deposition factor (X_{cl}), canister alloy/material, and decay heat load at time of analysis. The impact of each factor depends on the state of the canister, as summarized by Table 3-1. A brief discussion of each factor is provided in the subsections below.

Table 3-1. Summary of Canister Ranking Criteria [20, 50]

Parameter	Value	Canister Rank Value
Deposition Factor	$X_{cl} < 1.5$	+1
	$1.5 \leq X_{cl} < 2.5$	+2
	$2.5 \leq X_{cl} < 4$	+3
	$4 \leq X_{cl} < 5$	+4
	$X_{cl} \geq 5$	+5
Canister Alloy	316L(N)	0
	316	+1
	304L(N)	+2
	304	+3
Current Decay Heat Load (Horizontal Canisters)	>20 kW	0
	9 to 20 kW	+1
	< 9 kW	+2

3.1.1.1 Deposition Factor

The deposition factor, X_{cl}, is calculated through time using Equation (3-1) below. The deposition factor as shown is based on two main variables, the storage duration (*SD*, in years) and the atmospheric chloride level, which is captured by the ISFSI ranking, Z_{ISFSI} (distinguished from the canister ranking). Determining Z_{ISFSI} is thoroughly discussed in by EPRI [20], but for the purposes of this discussion, it's stated here that Z_{ISFSI} is a function of the mean absolute humidity and chlorides in the ISFSI environment. The impact of the chlorides on Z_{ISFSI} depends on site proximity to a marine shore as well as site elevation, cooling tower types (saline vs non-saline), and proximity of site to salted roads. The longer the storage duration and the higher the ISFSI rank, the larger the X_{cl} value.

$$X_{cl} = \frac{SD}{[(11 - Z_{ISFSI}) + \left(\frac{10}{Z_{ISFSI}}\right)]} \tag{3-1}$$

3.1.1.2 Canister Alloy

Impact of the canister material is based on a literature review of susceptibility. Lower carbon material is assigned a lower rank than high carbon material because it resists sensitization under typical manufacturing process. Sensitization becomes important because it can accelerate initiation of CISCC and can occur during welding processes [20]. According to EPRI [20], Type 316 alloys are ranked lower than Type 304 alloys because of the resistance to localized corrosion and SCC provided by the improved oxide layer resulting from the addition of molybdenum.

3.1.1.3 Decay Heat Load

Ranking values correlated with total heat decay are based on best-estimate thermal models. Ranking values depend on canister orientation, but only horizontal conditions are discussed here (ranking values for vertical canisters would change, but the analysis approach would be comparable). As the decay heat load of fuel diminishes with time, the canister surface will cool. Lower decay heats are thus associated with a higher

canister rank as lower temperatures can lead to deliquescence of deposited salts. EPRI noted in their studies that surfaces heated to more than 30°C above ambient do not deliquesce at all, and surfaces heated between 30°C and 25°C above ambient do not deliquesce for durations long enough to cause substantial risk for CISCC [20]. The ranking values shown in Table 3-1 reflect these effects.

3.1.2 Determination of Initiation Probability

The initiation probability threshold for each flaw in each modeled canister is randomly sampled from a uniform distribution between 0 and 1. The threshold is only sampled once per flaw position at each realization. The initiation probability of each canister, however, is assumed uniform across the surface of a canister. This initiation probability is modeled based on a canister's rank and is updated throughout the simulation. The initiation probability increases annually at an assumed rate (Δp_i), as determined by the canister's rank (Table 3-2). As the rank of a canister increases over time due to a decrease in decay heat load and increase in deposition factor, the assumed rate for increase in initiation probability per year is also adjusted. The initiation probability (P_{init}) by the end of a given time period is given by Equation (3-2), where Δt_{step} is the duration of each simulation time step (in units of '*years*') and *i* is the i^{th} time step.

$$P_{init} = 1 - \prod_{i=-1} (1 - \Delta p_i)^{\Delta t_{step}} \tag{3-2}$$

As mentioned above, the initiation probability is assumed uniform across the surface of a considered canister while the threshold can vary per each flaw considered on a canister as the thresholds are randomly sampled. Once the initiation probability reaches the sampled threshold for any potential flaw position, initiation of a crack occurs at that position. Given this approach of modeling the initiation probability with a randomized threshold, initiation for each flaw position occurs at a unique and random time. Incorporating the randomized threshold is more representative of realistic scenarios given that actual canisters do not have a uniform initiation probability across their surface.

Table 3-2. Assumed Values of Annual Increment in Initiation Probability for Each Canister Rank [50]

Canister Rank	Assumed Initiation Probability per Year
1	10^{-6}
2	5×10^{-6}
3	2×10^{-5}
4	10^{-4}
5	2×10^{-4}
6	5×10^{-4}
7	10^{-3}
8	2×10^{-3}
9	5×10^{-3}
10	0.01

3.2 Crack Growth

The crack growth rate model used in the analysis discussed here is the same approach that was used and discussed in EPRI's 2015 flaw growth assessment [20, 50]. Flaws of significant length do not result in canister rupture with this approach, thus the focus for crack growth is in the depth direction. Furthermore, additional growth of crack length after through-wall penetration at flaw sites is not considered. The main factors that influence the CGR model are ambient climate, canister surface temperature at the flaw location, and existing crack depth. Regarding the ambient climate and local surface temperature, crack growth only occurs when a RH threshold is surpassed at a flaw location, similar to the discussion in Section 2.2.3. The dependence of CGR on crack depth is modeled with two components split up by a transition where shallow crack

growth transitions to deep crack growth in order to capture a reduced growth rate as the crack evolves to a deep crack.

Crack growth is modeled as shown by Equation (3-3). The version presented here is a simplified version used in the actual modeling, where a dependence of the growth rate on stress intensity factor is not captured. The CGR coefficient is a function of depth and is sampled from a log-normal statistical distribution, once per flaw. To capture the transition between shallow and deep crack growth, a transition factor is also sampled from a log-normal distribution as shown in Table 3-3.

$$\frac{da}{dt} = \alpha \exp\left[-\frac{Q_g}{R}\left(\frac{1}{T} - \frac{1}{T_{ref}}\right)\right] for\ RH \geq RH_c\ and\ K_I > 0 \quad (3\text{-}3)$$

Where:

$\frac{da}{dt} =$ crack depth growth rate

$\alpha =$ CGR coefficient (mm/yr, and a function of crack depth)

$Q_g =$ crack growth activation energy (kJ/mole)

$R =$ universal gas constant (kJ/mole/K)

$T =$ surface temperature (K), obtained by measurement or analysis using Equation (3-4)

$T_{ref} =$ reference temperature for Arrhenius factor (K)

$K_I =$ stress intensity factor (MPa-m$^{0.5}$)

$RH =$ local relative humidity at surface (%), obtained from surface temperature and ambient humidity using Equation (3-5)

$RH_c =$ critical relative humidity of deposited chloride salts (%), given by Equation (3-6)

$$T(t) = T_{offset}(t) + \frac{1}{X}\sum_{i=0}^{X/\Delta t}[T_{atm}(t - X + i\Delta t_i)\Delta t_i] \quad (3\text{-}4)$$

$$RH(T,AH) = \frac{AH}{216.68}10^{-23.5581 + \left(\frac{2937.4}{T}\right)}T^{5.9283} \quad (3\text{-}5)$$

$$RH_c(T) = \frac{1}{100}[33.67 - 7.974 * 10^{-3}(T - 273.15) - 1.090 * 10^{-3}(T - 273.15)^2] - RH_\Delta \quad (3\text{-}6)$$

Inputs to the CGR model described between Equations (3-3) and (3-6) are all shown in Table 3-3. In the thermal model described by Equation (3-4), the local ambient temperature (T_{atm}) is offset with a chosen temperature (T_{offset}) to account for the canister thermal heat load to produce the local temperature at a flaw position. Time-series data from the National Oceanic and Atmospheric Administration (NOAA) is used to determine an average on the ambient temperature over a year in Equation (3-4). For cases modeling canisters of the same Z_{ISFSI}, the same climate data is used over all canisters. For cases considering multiple Z_{ISFSI} in a single realization, different NOAA climate data is sampled for corresponding ranges of each ZISFS. The local temperature is then used along with absolute humidity to calculate a relative humidity as shown in Equation (3-5, while equation (3-6) shows how the critical RH is calculated.

Table 3-3. Crack Growth Rate Inputs [50].

Variable	Description	Units	Base Case Value	
Q_g	CGR activation energy	kJ/mol	40.0	
R	Universal gas constant	kJ/mol/K	0.008314	
T_{ref}	Arrhenius relationship reference temperature	K	353.15	
$\alpha_{shallow}$	Shallow crack growth rate coefficient at the reference temperature	mm/yr	Distribution Type	Log-Norm.
			Log-μ	2.39
			Log-σ	1.66
			Min	0.01
			Max	500
$\alpha_{shallow}/a_{deep}$	Shallow to deep crack growth transition factor	-	Distribution Type	Log-Norm.
			Log-μ	-3.54
			Log-σ	2.21
			Min	0.0003
			Max	1.0
a_0	Initial depth of crack at time of initiation	mm	Distribution Type	Normal
			μ	0.5
			σ	1.0
			Min	0.01
			Max	1.0
a_{trans}	Depth at which CGR coefficient transition occurs	mm	Distribution Type	Normal
			μ	2.235
			σ	0.561
			Min	0.1
			Max	12.0
X	Period of moving average for assessing climate data	hr	6.0	
$T_{offset,0}$	Initial surface temperature offset relative to ambient conditions	K	Distribution Type	Uniform
			Min	0.0
			Max	35.0
RH_Δ	Relative humidity offset for corrosion below the DRH curve for $MgCl_2$	-	0.07	
AH	Hourly data for ambient absolute humidity	g/m^3	See Section A.3.2.3	
T_{atm}	Hourly data for ambient temperature	K		

3.3 Inspections

Inspections are modeled in a two-step process and are handled on a flaw-by-flaw basis with independent sampling of detectability for each flaw. The first step in the process checks for the presence of corrosion, and the second inspection searches for the presence of a stress corrosion *crack* only after having detected corrosion degradation in the first inspection. At each initiated flaw within the simulation, three possible outcomes exist for an inspection:

1. Nothing of significance is found
2. Corrosion is identified but a crack is not detected
3. A crack is detected, sized, and compared against a predetermined critical length. If a flaw size is less than the critical length, the simulation continues and the crack is allowed to grow over time. If a crack is detected but the flaw size measurement is greater than the specified threshold for acceptability, the growth of the detected crack is halted. The simulation then considers that flaw as repaired and is not allowed to propagate through-wall.

Figure 3-2 provides a graphical representation of the canister inspection logic. Inspection samples can be executed using two different approaches. In the first approach, a sample can be a specified number of canisters chosen at random. In the second approach, a sample is chosen based on a minimum canister rank in a realization, where a specified number of canisters is specified within the constrained batch. In the case where inspections are performed on a specified number of random canisters, a different canister set of canisters is set to be inspected at each inspection. If corrosion degradation is detected at any point, the scope of inspection is expanded to all of the canisters in the realization. In the case where ranking criteria is used in a set of canisters with mixed susceptibility, if corrosion is detected in the batch of specified inspections, the sample size is expanded to all canisters above the rank of the detected canister minus 2. For example, if a canister of rank 7 tests positive for corrosion, then all canisters above a rank of 5 are inspected for corrosion.

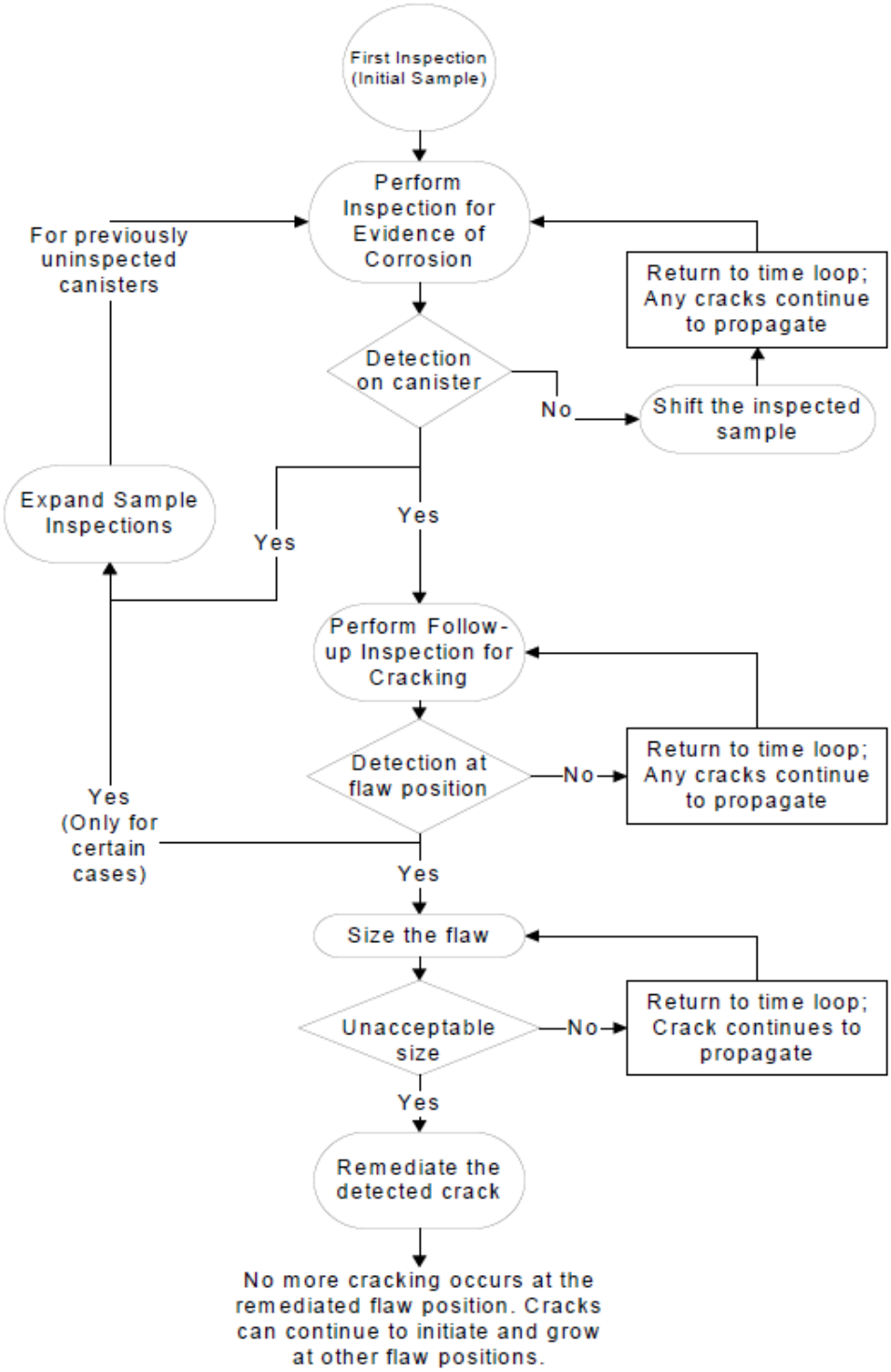

Figure 3-2. Flow chart for inspection logic [50].

As inspection of a canister for corrosion is executed on a flaw-by-flaw basis, detectability is carried out by independent sampling per flaw. The input factors affecting detectability of a flaw are (1) inspection-coverage ($f_{cov,}$ which represents the likelihood that a flaw position on a canister is within the inspection coverage area) and (2) probability of detection (*POD*). As the initial inspection is for corrosion only, this *POD* is independent of flaw size. With f_{cov} and *POD* as inputs (constants) to the model, an examination is simulated by randomly sampling a value between 0 and 1 (for both f_{cov} and *POD*) from a uniform distribution for each flaw position. If the sampled value corresponding to coverage is less than f_{cov} , the flaw is considered for inspection. If a flaw is considered for inspection, a second value is sampled and compared to the input *POD*. When the input *POD* is greater than this second sampled value, corrosion is considered detected at that flaw location. Inspection for cracks following detection of corrosion is executed in a similar fashion. The main difference in the crack approach is that *POD* is not a single input value but is rather represented by a curve that correlates flaw size with detectability; *POD* for cracks starts at 0% and increases with increasing crack size. Lastly, to simulate areas that might be inaccessible to inspect due to geometric constraints, a fraction of potential flaw positions are assigned a *POD* of zero. These uninspected cracks are thus allowed to propagate until the end of the simulation with a higher likelihood of becoming through-wall. For cracks detected using the aforementioned approach, remediation only occurs if the crack is larger than an input size threshold. These detected and remediated cracks are then halted from growth and the simulation tags these flaws as repaired. Propagate of these remediated cracks is not allowed for the remainder of the simulation.

3.4 Presentation of Results

Analysis results are presented using a cumulative probability of leakage (CPL). The CPL is calculated as demonstrated by Equation (3-7) below,

$$CPL = \frac{1}{N_{real} N_{can}} \sum_{t_{start}}^{t_{end}} \begin{pmatrix} Number\ of\ canisters\ across\ all\ realizations\ with \\ the\ first\ leaking\ crack\ during\ this\ type\ perod \end{pmatrix} \qquad (3\text{-}7)$$

Where:

$t_{start} =$ start of time period of interest (yr)

$t_{end} =$ time of last time step of the simulation (yr)

$N_{real} =$ number of realizations

$N_{can} =$ number of canisters per realization

As calculated, the CPL conveys the average probability of a canister developing the first through-wall crack during a time period of interest [20, 50]. CPL can be a reliable metric to assess likelihood of CISCC since CPL is expected to converge for a set of modeled conditions as larger values of N_{real} are used.

4 SUMMARY AND CONCLUSIONS

This report documents a scoping study that identifies and compiles the current state of knowledge on the susceptibility of dry storage systems for spent nuclear fuel to CISCC. It compiled the existing data and models necessary to provide an assessment of data gaps to validate and verify mechanistic, or hybrid mechanistic/probabilistic, sub-models to predict canister performance. Sections 2 and 3 discussed how mechanistic models can be used for phenomena where models can be parameterized, and probabilistic approaches can be taken for processes that cannot be deterministically modeled or where uncertainty exists in the parameterization. This combination of approaches allows uncertainty to be captured in the modeling, whether that's due to inherent randomness in some of the stochastic processes, or whether it's due to an incomplete understanding of adequate parameters in the modeling. The modeling approaches discussed in this report highlight essential models needed to inform the likelihood and timing of CISCC. The global phenomena identified as essential to inform likelihood and timing of CISCC are: corrosion initiation, crack initiation, crack growth, and crack mitigation if inspections that lead to repairs are to be modeled. Models to capture each of these phenomena summarize as follows:

- Corrosion and Crack Initiation
    - Different approaches can be taken to model initiation of a crack. A stochastic approach can be taken such as EPRI did in their work, which relies on estimating a crack initiation probability that is dependent on canister conditions [50]. The crack initiation probability should be informed and guided by realistic scenarios as EPRI does. Alternatively, a mechanistic approach can be taken such as SNL has previously considered where corrosion in the form of pitting is a precursor to crack initiation. With this mechanistic approach, initiation of corrosion is modeled based on local RH reaching a critical value at considered flaw positions. Calculating local RH on canister locations depends on environmental as well as canister thermodynamics. For corrosion initiation, key parameters needed therefore include: a canister thermal model and a weather model (ambient absolute humidity and temperature). Transition from a pit to a crack depends on a second model that considers the stress distribution in a pit (Kondo approach [46, 47]) which requires its own parameterization. The stress distribution is modeled based on a maximum possible pit size for a given brine composition, but salt deposition rates have to be known for considered locations to determine

brine composition. As implemented in the SNL model, the transition from pit to crack also depends on a critical stress intensity factor that determines the transitional point, but values for this parameter vary in the literature so a probabilistic approach has to be incorporated to capture the uncertainty on crack initiation.

- Crack Growth
    - Once a crack initiates, properly modeling its growth over time becomes important. In reality, crack growth rate is dependent on many parameters that include: temperature, local stress distribution, present chlorides, and material yield stress. However, modeling of crack growth is commonly performed with the Wu and Modarres model (Equation (2-2)) [49]. The Wu and Modarres approach simplifies crack growth to be a function of temperature and a calculated crack tip stress intensity factor. The approach results in crack growth rate that is dependent on two primary components: (1) an Arrhenius relationship that is a function of temperature and, (2) a power-law relationship that's a function of the crack tip stress intensity factor. Parameters in this relationship, however, have to be obtained from literature for relevant conditions or calibrated from experimental data. Calibrations with experimental data have more commonly been performed using measured data for crack growth under atmospheric conditions. However, Bryan *et al.* have noted that confidence has risen in using data from experiments where growth rates are measured on samples immersed in solutions that mimic marine environments [12, 21].
- Inspection
    - Inspections on canisters can identify cracks that should be repaired to mitigate SCC. Inspections on canisters can be modeled to closely represent actual inspections. Controlling the scope of inspections can be based on randomized and specified sample sizes or on different criteria that consider the known site or canister conditions. EPRI, for example, incorporates a ranking criterion in their approach to modeling inspections [50]. If inspections are considered in a risk assessment, relevant parameters for modeling inspections for canisters can include: probability of detection, inspection coverage, and critical crack lengths that can trigger repairs on canisters to halt crack growth.

Based on the provided summaries, mechanistic or hybrid mechanistic/probabilistic sub-models are recommended to inform the likelihood and timing of CISCC when possible. The validated models will aid in risk-informing aging management and inspection. However, any models used need to be calibrated and/or validated with experimental data to properly inform CISCC. Based on the overview presented in this report, the SNL model can be leveraged as a tool to inform initiation of CISCC. The inherent mechanistically-based sub-models for the stages described above allow the SNL model to cover a range of scenarios to inform CISCC. However, the model does contain simplifications based on lack of data or mechanistic basis, and improving upon these existing gaps can help reduce model uncertainty. Identified gaps can be summarized as follows:

- For corrosion initiation, the approach SNL has taken can be useful if reliable weather, salt deposition, and canister thermal sub-models are used. Currently, salt deposition is handled at a constant rate in the SNL model, but improvements to this parameter could account for different site locations to result in a more robust model.
- For pit to crack transitions, the current implementation allows for cracks to initiate based on a prescribed critical stress intensity factor (Kondo criterion). However, work is still needed to reliably parameterize use of the Kondo criterion for CISCC since uncertainty exists for some of its input parameters in its current implementation. More data on transition points is needed to reduce the uncertainty since the existing data is scarce.
- For crack growth, the implemented Wu and Modarres sub-model has wide acceptance in the literature. However, prior calibrations have been performed using literature and experimental data for specimens under atmospheric conditions. Improvements to the calibration of this model for CISCC in stainless steel are underway as more experimental data is acquired for crack growth in specimens under immersed conditions (under a solution representing marine environments), and this data is expected to further improve confidence for crack growth in stainless steel canisters.
- The thermal sub-model used is limited for a canister with a heat load that starts at 24 kW and decays to 2 kW over 292 years. Expansion to higher initial heat loads is needed to capture a broader range of scenarios.
- A capability that is not currently implemented in the SNL model is an ability to simulate canister inspections and repair a crack if an inspection were to detect a crack beyond acceptable. However, the probabilistic approach taken by EPRI demonstrated to be a viable implementation to capture inspections and halt growth as a way of simulating repairs. Adding this capability can render more realistic predictions for sites that consider periodic inspections.
- While concerted efforts have been taken to validate the sub-models in the SNL tool, rigorous efforts to compare model predictions for timing through-wall cracking against operating experience data have not been accomplished. Such comparisons are challenging because comprehensive data encompassing inspections and corresponding consequence for CISCC on canisters was not found in the literature. However, verifying predictions may be possible in an

indirect way. For example, EPRI, has compared their methodology against cracks observed on stainless steel system components for three different events: Refueling water storage tank at Koeberg Nuclear Power Station Unit 2, emergency core cooling system piping at St. Lucie Unit 2, and safety injection system piping at Koeberg Nuclear Power Station. A similar approach can be considered for the SNL model.

As is, the SNL model can simulate CISCC progression for canisters in a mechanistic-probabilistic way. If adequate calibration and parameterization for the aforementioned mechanistic sub-models can be achieved, and if they are combined with a capability to simulate inspections/repairs, a more comprehensive perspective to inform the likelihood and timing of CISCC can be achieved. To give further confidence to the model, validation from either operating experience (or comparable) data should be sought out.

5 REFERENCES

[1] NRC, "Storage of Spent Nuclear Fuel," 3 May 2021. [Online]. Available: https://www.nrc.gov/waste/spent-fuel-storage.html. [Accessed 6 July 2021].

[2] NRC, *10 CFR Part 72-Licensing Requirements for the Independent Storage of Spent Nuclear Fuel, High-Level Radioactive Waster, and Reactor-Related Greater than Class C Waste,* Washington DC, September 2020. www.nrc.gov/reading-rm/doc-collections/cfr/part072/.

[3] NRC, *Regulatory Guide 3.50-Standard Format and Content for a Specific License Application for an Independent Spent Fuel Storage Installation or Monitored Retrievable Storage Facility,* Washington DC, 2014. www.nrc.gov/docs/ML1404/ML14043A080.pdf.

[4] NRC, *Regulatory Guide 3.62-Standard Review Plan for Spent Fuel Dry Storage Systems at a General License Facility,* Washington DC, 2014. www.nrc.gov/docs/ML0037/ML003739545.pdf.

[5] J. J. Lichtenwalter, S. M. Bowman, M. D. DeHart and C. M. Hopper, "Criticality Benchmark Guide for Light Water Reactor Fuel in Transportation and Storage Packages," NUREG/CR-6361 ORNL/TM-13211, SNL, Washington DC, 1997. www.nrc.gov/docs/ML0108/ML010820352.pdf.

[6] S. M. Bowman, I. C. Gauld and J. C. Wagner, "Recommendations on Fuel Parameters for Standard Technical Specifications for Spent Fuel Storage Casks," NUREG/CR-6716 ORNL/TM-2000/385, NRC and ORNL, Washington DC, March 2001. www.nrg.gov/docs/ML0108/ML010820352.pdf.

[7] NRC, "Standard Review Plan for Spent Fuel Dry Storage Facilities," NUREG-1567, Washington DC, 2020. www.nrc.gov/docs/ML0036/ML003686776.pdf.

[8] NRC, "Aging Management of Nuclear Power Plant Containments for License Renewal -- NUREG-1611," U.S. Nuclear Regulatory Comission, 1995.

[9] United Sates Nuclear Regulatory Commission, "Standard Review Plan for Renewal of Specific Licenses and Certificates of Compliance for Dry Storage of Spent Nuclear Fuel -- NUREG-1927," NRC, Washington, DC, 2016.

[10] United Sates Nuclear Regulatory Commission, "Managing Aging Processes in Storage (MAPS) Report -- NUREG-2214," NRC, Washington, DC, 2019.

[11] NRC, "Typical Dry Cask Storage System," U.S. NRC, 2020 08 07. [Online]. Available: https://www.nrc.gov/waste/spent-fuel-storage/diagram-typical-dry-cask-system.html. [Accessed 13 06 2022].

[12] C. Bryan, R. Schaller, R. Katona, D. Brooks and L. Gilkey, "Using SCC Probabilistic Model Uncertainties to Drive Experimental Research," in *Spent Fuel and Waste Science and Technology (SFWST)*, 2022.

[13] C. Bryan, A. Knight, B. Nation, T. Montoya, E. Karasz, R. Katona and R. Schaller, "FY21 Status Report: SNF Interim Storage Canister Corrosion and Surface Environment Investigations," Sandia National Laboratories, 2021.

[14] Kain, "Marine Atmospheric Stress Corrosion Cracking of Austenitic Stainless Steels," *Materials Performance,* vol. 29, no. 12, pp. 60-62, December 1990.

[15] R. Schaller, A. Knight, C. Bryan, B. Nation, T. Montoya and R. Katona, "FY20 Status Report: SNF Interim Storage Canister Corrosion and Surface Environment Investigations, SAND2020-12663R," Sandia National Laboraries, 2020.

[16] EPRI, "Calvert Cliffs Stainless Steel Dry Storage Canister Inspection," p. 460, 2014.

[17] C. Bryan and D. Enos, "Analysis of Dust Samples Collected from Spent Nuclear Fuel Interim Storage Containers at Hope Creek, Delaware, and Diablo Canyon, California," SAND2014-16383, Sandia National Laboratories, p. 281, 2014.

[18] C. Bryan and D. Enos, "Analysis of Dust Samples Collected from an In-Service Interim Storage System at the Maine Yankee Nuclear Site," SAND2016-10266, Sandia National Laboratories, p. 51, 2016.

[19] C. Bryan and E. Schindelholz, "Analysis of Samples Collected from the Surface of Interim Storage Canisters at Calvert Cliffs in June, 2017: Revision 01," SAND2017-12429, Sandia National Laboratories, p. 26, 2017.

[20] EPRI, "Susceptibility Assessment Criteria for Chloride-Induced Stress Corrosion Cracking (CISCC) of Welded Stainless Steel Canisters for Dry Cask Storage Systems," Electric Power Research Institute, 2015.

[21] N. W. Porter, D. Brooks, C. Bryan, R. Katona and R. Schaller, "FY21 Status Report: Proabilistic SCC Model for SNF Dry Storage Canisters SAND2021-9213R," Sandia National Laboratories, 2021.

[22] NRC, "Finite Element Analysis of Weld Residual Stresses in Austenitic Stainless Steel Dry Cask Storage System Canisters," NRC Technical Letter Report (ADAMS ML13330A512). Nuclear Regulatory Commission, 2013.

[23] D. Enos and C. Bryan, "Final Report: Characterization of Canister Mockup Weld Residual Stresses," FCRD-UFD-2016-000064, U.S. DOE, 2016.

[24] L. Caseres and T. S. Mintz, "Atmospheric Stress Corrosion Cracking Susceptibility of Welded and Unwelded 304, 304L, and 316L Austenitic Stainless Steels Commonly Used for Dry Cask Storage Containers Exposed to Marine Environments," U.S. NRC, 2010.

[25] EPRI, "Assessment of Stress Corrosion Cracking Susceptibility for Stainless Steels Exposed to Atmospheric Chloride and Non-Chloride Salts," Electric Power Research Institute, 2014.

[26] R. Dingreville, C. J. Sallaberry, C. R. Bryan, C. Stockman, H. Adkins and M. Sutton, "Uncertainty Quantification Methodologies Development for Storage and Transportation of Used Nuclear Fuel: Pilot Study on Stress Corrosion Cracking of Canister Welds," OUO/ECI SAND2014-19467, SNL, Albuquerque NM, 2014.

[27] C. R. Bryan, C. J. Sallaberry, R. Dingreville, C. T. Stockman, H. Adkins and M. Sutton, "Probabilistic Performance Assessment: SCC of SNF Interim Storage Canisters," in *Proceedings of the International High-Level Radioactive Waste Management (IHLRWM) Conference*, Charleston SC, April 2015.

[28] R. Dingreville and C. R. Bryan, "Uncertainty Quantification Methodologies Development for Stress Corrosion Crack of Canister Welds," SAND2016-9487R, SNL, Albuquerque NM, 2016.

[29] C. J. O'Brien, C. Alexander, C. R. Bryan, E. J. Schindelholz and R. Dingreville, "Status Report: Uncertainty Quantification of Environmentally Assisted Stress

Corrosion Cracking in Used Fuel Canisters," SAND2019-3600R, SNL, Albuquerque NM, 2019.

[30] E. Schindelholz, R. G. Kelly, I. S. Cole, W. D. Ganther and T. H. Muster, "Comparability and Accuracy of Time of Wetness Sensing Methods Relevant for Atmospheric Corrosion," *Corrosion Science,* vol. 67, pp. 233-241, February 2013. doi: 10.1016/j.corsci.2012.10.026.

[31] A. Turnbull, L. McCartney and S. Zhou, "A model to predict the evolution of pitting corrosion and the pit-to-crack transition incorporating statistically distributed input parameters," *Corrosion Science,* vol. 48, no. 8, pp. 2084-2105, 2006.

[32] C. Bryan, A. Knight, R. Katona, A. Sanchez, E. Schindelholz and R. Schaller, "Physical and chemical properties of sea salt deliquescent brines as a function of temperature and relative humidity," *Science of the Total Environment,* vol. 824, no. 154462, 2022.

[33] S. Suffield, J. A. Fort, J. M. Cuta and H. E. Adkins, "Thermal Modeling of NUHOMS HSM15 Stortage Module at Calvert Cliffs Nuclear Power Station ISFSI," U.S. Department of Energy, 2012.

[34] W. Wagner and A. Prub, "The IAPWS forumatoion 1995 for the thermodynamic properties of orginary water substance for general and scientific use," *Journal of physical and Chemical Reference Data,* vol. 31, no. 2, pp. 387-535, 2002.

[35] A. e. a. Nishikata, "An electrochemical impedance study on atmospheric corrosion of steels in a cyclic wet-dry condition," *Corrosion Science,* vol. 37, no. 12, pp. 2059-2069, 1995.

[36] J. Siegel, M. Schindelholz and F. Friedersdorf, "Small Scale Crack Growth Sensor for Determination of AA5XXX Susceptibility to SCC," in *CORROSION*, 2015.

[37] NRC, "Assessment of Stress Corrosion Cracking Susceptibility for Austentitic Strainless Steels Exposed to Atmospheric Chloride and Non-Chloride Salts," U.S. Nuclear Regulatory Commision, Washington D.C., 2014.

[38] T. D. Weirich, J. Srinivasan, J. M. Taylor, M. A. Melia, P. J. Noell, C. R. Bryan, G. S. Frankel, J. S. Locke and E. J. Schindelholz, "Humidy Effects on Pitting of Ground Stainless Exposed to Sea Salt Particles," *Journal of the Electrochemical Society,* vol. 166, no. 11, pp. C3477-C3487, 2019.

[39] J. Srinivasan, T. D. Weirich, G. A. Marino, A. R. Annerino, J. M. Taylor, P. J. Noell, J. J. Griego, R. F. Schaller, C. R. Bryan, J. S. Locke and E. J. Schindelholz, "Long-Term Effects of Humidity on Stainless Steel Pitting in Sea Salt Exposures," *Journal of the Electrochemical Society,* vol. 168, no. 021501, 2021.

[40] Z. Y. Chen and R. G. Kelly, "Computational Modeling of Bounding Conditions for Pit Size on Stainless Steel in Atmospheric Environments," *Journal of the Electrochemical Society,* vol. 157, no. 2, p. C69, 2010. doi:10.1149/1.3261803.

[41] J. Srinivasan and R. G. Kelly, "On a Recent Quantiative Framework Examining the Critical Factors for Localized Corrosion and Its Impact on the Galvele Pit Stability Criterion," *Corrosion,* vol. 73, pp. 613-633, 2017. doi: 10.5006/2334.

[42] Z. Y. Chen, F. Cui and R. G. Kelly, "Calculations of Cathodic Current Delivery Capacity and Stability of Crevice Corrosion Under Atmospheric Environments," *Journal of the Electrochemical Society,* vol. 155, no. 7, pp. C360-C368., May 2008. doi:10.1149/1.2926557.

[43] M. Woldemedhin, J. Srinivasan and R. Kelly, "Effects of environmental factors on key kinetic parameters relevant to pitting corrosion.," *Journal of Solid State Electrochemistry,* vol. 19, pp. 3449-3461, 2015.

[44] M. Woldemedhin, M. Shedd and R. Kelly, "Evaluation of the maximum pit size model on stainless steels under thin film electrolyte conditions.," *Journal of Solid State Electrochemistry,* vol. 161, pp. E3216-E3224, 2014.

[45] J. Srinivasan, M. McGrath and R. Kelly, "A High-Throughput Artificial Pit Technique to Measure Kinetic Parameters for PItting Stability," *Journal of the Electrochemical Society,* vol. 162, pp. C725-C731, 2015.

[46] C. R. Bryan, R. P. Dingreville and D. E. Weirich, "A probabilistic Model for Stress Corrosion Cracking of Stainless Steel SNF Interim Storage Canisters," in *18th International Symposium on the Packaging and Transportation of Radioactive Materials (PATRAM)*, Kobe, Japan, 2016.

[47] Y. Kondo, "Prediction of fatigue crack initiation life based on pit growth.," *CORROSION,* vol. 45, pp. 7-11, 1989.

[48] C. Bryan and D. Enos, "Summary of available data for estimating chloride-induced SCC crack growth rates for 304/316 stainless steel," Sandia National Labs, 2016.

[49] G. Wu and M. Modarres, "A Probabilistic-Mechanistic Approach to Modeling STress Corrosion Cracking in Allow 600 Components with Applications," in *PSAM*, 2012.

[50] EPRI, "Aging Management Guidance to Address Potential Chloride-Induced Stress Corrosion Cracking of Welded Stainless Steel Canisters - 3002008193," Electric Power Research Institute, 2017.

[51] EPRI, "Susceptibility Assessment Criteria for Chloride-Induced Stress Corrosion Cracking (CISCC) of Welded Stainless Steel Canisters for Dry Cask Storage Systems," EPRI, Palo Alto, 2015.